Supporting Information

Benzophenone Ultrafast Triplet Population: Revisiting the Kinetic Model by Surface Hopping Dynamics

Marco Marazzi,[†§] Sebastian Mai,[‡] Leticia González,[‡] Daniel Roca-Sanjuán,[∥] Mickaël G. Delcey,[⊥] Roland Lindh,[⊥┤] and Antonio Monari*[†§]*

[†] Théorie-Modélisation-Simulation, Université de Lorraine − Nancy, SRSMC Boulevard des Aiguillettes, Vandoeuvre-lès-Nancy, Nancy, France
[§] Théorie-Modélisation-Simulation, CNRS, SRSMC Boulevard des Aiguillettes, Vandoeuvre-lès-Nancy, Nancy, France
[‡] Institute of Theoretical Chemistry, University of Vienna, Währinger Straße 17, A-1090 Vienna, Austria
[∥] Instituto de Ciencia Molecular, Universitat de València, P. O. Box 22085, ES-46071 València, Spain
[⊥] Department of Chemistry–Ångstrom Laboratory, Uppsala University, Uppsala 751 05, Sweden
[┤] Uppsala Center of Computational Chemistry - UC$_3$, Uppsala University, Uppsala 751 05, Sweden

Content

1. Computational Details
2. Kinetic Models Parameters
3. Single Point Calculations of Geometries Along the Potential Energy Surface
4. Wavefunction Amplitude Graphs of the 39 Trajectories Populating the Triplet Manifold
5. Geometrical Analysis of the 39 Trajectories Populating the Triplet Manifold
6. Franck−Condon Structure at the CASSCF(12,11)/ANO-S-VDZP Level of Theory
7. Description of the Transient Absorption Spectrum Simulation
8. References

1. Computational Details

In this study, the *ab-initio* multiconfigurational quantum chemistry method CASSCF (Complete Active Space Self Consistent Field)[S1] as implemented in MOLCAS 8[S2] was employed, averaging over the lowest-lying 3 singlet or triplet states (SA-3-CASSCF). The calculation of several energy gradients is necessary for each step of each trajectory. The analytical gradients of each state in an interval of 0.25 eV from the active state were calculated in parallel and the Cholesky decomposition was used to approximate the two-electron integrals, in order to significantly reduce the computational effort (by *ca.* a factor 3 on our local linux cluster based at the Université de Lorraine).

Spin-orbit couplings were calculated based on the SA-CASSCF wavefunctions using the RASSI module of MOLCAS, which calculates spin-orbit matrix elements according to the AMFI (atomic mean field integrals) formalism.[S3] The values of the spin-orbit coupling elements were found to be of the order of 20 cm^{-1}, in agreement with previous computational studies (see ref. 21 in the main text).

65 initial conditions (Cartesian coordinates and atomic velocities) were generated by sampling from a Wigner distribution.[S4,S5] As input, a set of vibrational frequencies and the corresponding normal mode vectors were provided by a frequency calculation performed on the Franck–Condon geometry at the CASSCF(12,11)/ANO-S-VDZP level of theory. The calculated kinetic and potential contributions to the total energy are of the same order: the kinetic energy is 0.087 ± 0.019 a.u. and the potential energy is 0.099 ± 0.019 a.u.

A 0.5 fs time step was selected for each trajectory, while the electronic wavefunctions were propagated with a 0.02 fs step. The dynamic was run in the full diagonal representation including non-adiabatic and spin-orbit coupling using the SHARC code.[S6] To calculate the non-adiabatic interaction between the different states we considered the wavefunction overlaps $\langle \psi_\alpha(t_0) | \psi_\beta(t) \rangle$, within the local diabatization formalism.[S7] The spin-orbit couplings were explicitly calculated at each time step, considering all multiplet components. During the dynamics, the velocity is rescaled to adjust the kinetic energy after a surface hop and energy-based electronic decoherence correction with a parameter of 0.1 Hartree[S8] was applied.

On the one hand, we note that more sophisticated electronic decoherence corrections are available.[S9-S12] Nevertheless, they are adding significant extra cost to the simulations or require considerable implementation effort. On the other hand, the Granucci–Persico algorithm[S8] is a conceptually and computationally simple means of estimating electronic decoherence, and we therefore used it.

All details concerning the SHARC code can be found at https://sharc-md.org.

2. Kinetic Models Parameters

Two kinetic models were applied, called parallel and serial kinetic models. The parallel model takes into account the simultaneous formation of T_1 and T_2 from S_1, as shown by the surface hopping dynamics study, and it is formulated as follows:

$$S_1(t) = e^{-(k_1+k_2)t}$$

$$T_1(t) = \frac{k_1}{k_1+k_2} - \frac{k_1}{k_1+k_2} e^{-(k_1+k_2)t}$$

$$T_2(t) = \frac{k_2}{k_1+k_2} - \frac{k_2}{k_1+k_2} e^{-(k_1+k_2)t}$$

$$\tau_{T1} = \frac{1}{k_1} = 897\,fs$$

$$\tau_{T2} = \frac{1}{k_2} = 3383\,fs$$

$$\tau_{S1} = \frac{1}{\frac{1}{\tau_{T1}} + \frac{1}{\tau_{T2}}} = 709\,fs$$

where *t* is time, *k* is the rate constant value and τ is the lifetime value.
The serial kinetic model considers the formation of either T_1 or T_2 (or T_3) from S_1, as usually postulated in the fitting procedures of the transient absorption experimental data, based on signal strengths. It can be formulated as follows:

$$S_1(t) = e^{-\frac{t}{\tau_{S1}}}$$

$$T_1(t) = 1 - e^{-\frac{t}{\tau_{T1}}}$$

$$T_2(t) = 1 - e^{-\frac{t}{\tau_{T2}}}$$

$$\tau_{T1} = 1004\,fs$$

$$\tau_{T2} = 4465\,fs$$

$$\tau_{S1} = 683\,fs$$

For the serial kinetic model, a full decomposition of the triplet contribution is given in Figure S1. Moreover, all lifetime values and relative fitting errors are given in Table S1, including the contribution from the singlet low-lying excited state.

As can be seen, the sum of T_1 and T_2 contributions accounts for the whole intersystem crossing process, while T_3 can be neglected.

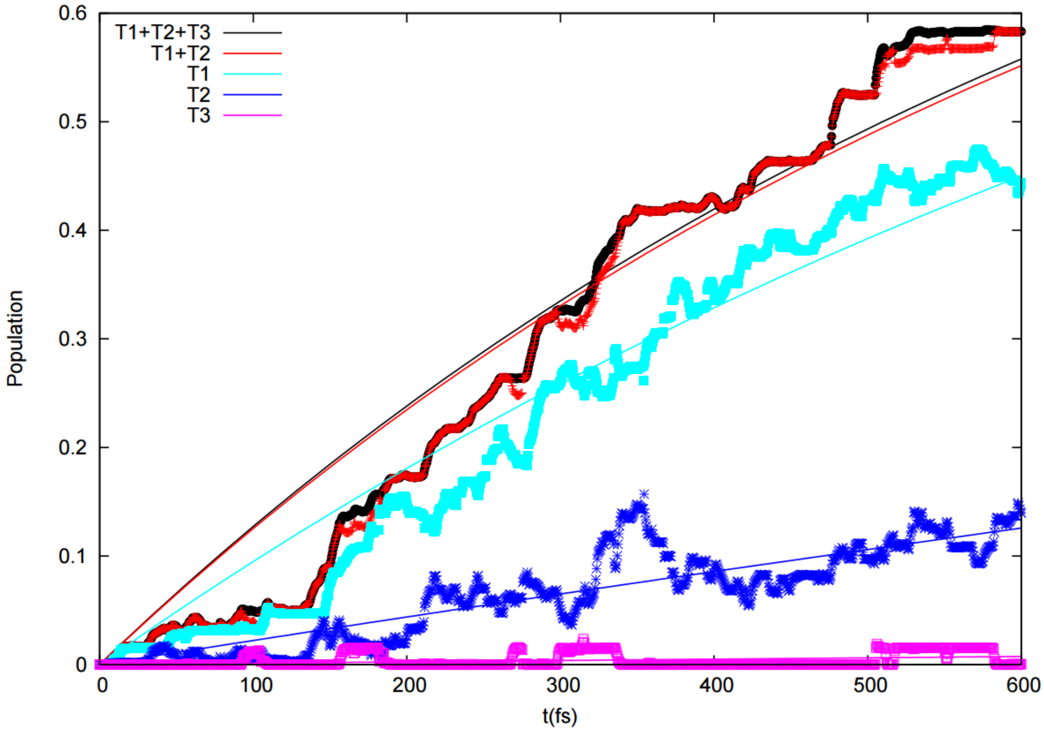

Figure S1. Global fitting to a single exponential rate law for T_1, T_2, T_3, and their sum.

Table S1. Serial kinetic model: lifetime values τ and relative fitting errors for S_1, T_1, T_2, T_3, and the sum of the triplet contributions.

Electronic state	τ (fs)	Δτ (fs)	Δτ (%)
S_1	683	3.8	0.55
T_1	1004	4.8	0.48
T_2	4465	36.2	0.81
$T_1 + T_2$	747	4.0	0.54
$T_1 + T_2 + T_3$	735	4.0	0.54

For the parallel kinetic model, the rate constant values and relative fitting errors are given in Table S2.

Table S2. Parallel kinetic model: rate constant values and relative fitting errors for the $S_1 \rightarrow T_1$ (k_1) and $S_1 \rightarrow T_2$ (k_2) pathways.

Pathway	k (fs^{-1})	Δk (fs^{-1})	Δk (%)
$S_1 \rightarrow T_1$	0.00111531	$1.129 \cdot 10^{-5}$	1.01
$S_1 \rightarrow T_2$	0.00029563	$1.002 \cdot 10^{-5}$	3.39

It should be noted that the relative fitting errors shown in Tables S1 and S2 take into account the collected data from the sampled trajectories, but do not include the systematic errors due to the chosen level of theory and to the applied surface hopping algorithm.

A comparison of the two proposed kinetic models up to 5 ps is shown in Figure S2a,b. As it can be seen (also in Figure 1 of the main text) the two curves almost coincide up to 600 fs, while the population plateau for the triplet states is reached at larger times for the serial kinetic model. Nevertheless, while the overall population of the theoretically oriented parallel model adds up to one, this is not the case for the experimentally oriented serial model. Indeed, the serial model is intended to reproduce the experimental fitting of signal strength that (unlike the overall population) does not have to add up to one.

In order to get a deeper insight into the singlet-triplet and triplet-triplet transitions, Figure S2c shows net transfers between couples of electronic excited states, based on the number of hopping events recorded along the trajectories. We found, confirming our models, net transfers from S_1 to both T_1 and T_2, with a slight preference for the $S_1 \longrightarrow T_2$ channel, *i.e.* the indirect mechanism. Once the triplet manifold is populated, an equilibrium is established between T_1 and T_2 states, with a net transfer (14 hops) from T_2 and T_1, indicating an emerging equilibrium (the number of $T_1 \longrightarrow T_2$ and $T_2 \longrightarrow T_1$ hops is comparable but not identical, since the equilibrium first has to be established).

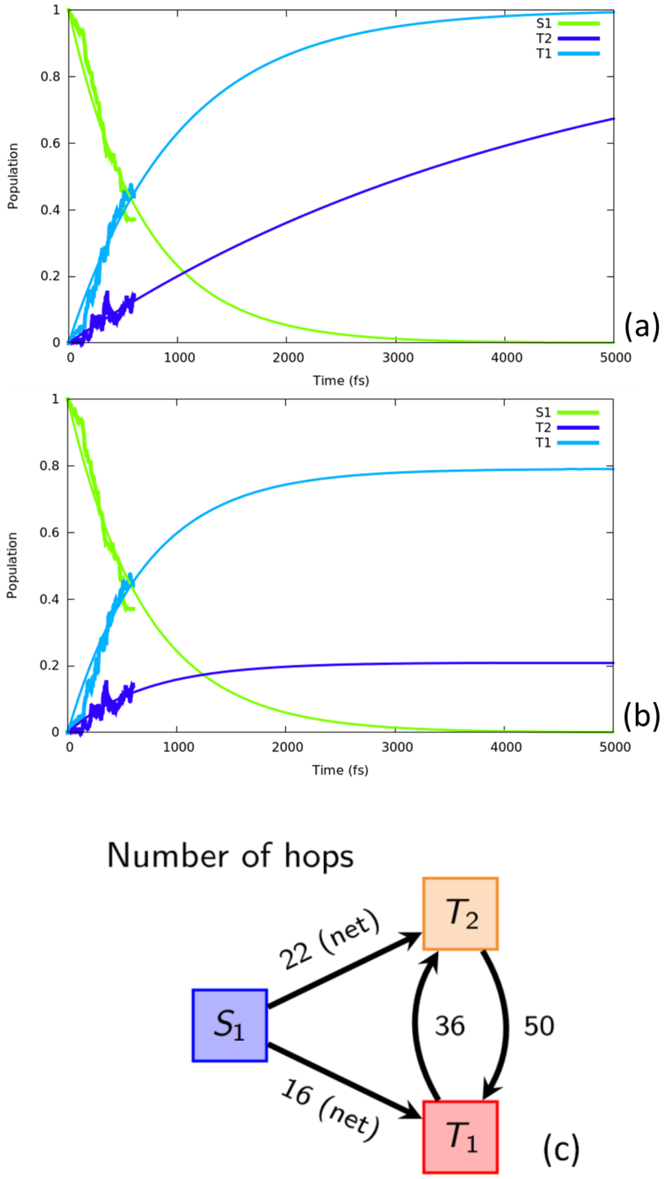

Figure S2. Serial (a) and parallel (b) kinetic models including the dynamics data for the first 600 fs and the analytical curves up to 5 ps. Scheme of the net transfers between S_1, T_1 and T_2 electronic states, based on the number of hopping events: 86 $S_1 \rightarrow T_1$ hops, 70 $T_1 \rightarrow S_1$ hops, 349 $S_1 \rightarrow T_2$ hops, 327 $T_2 \rightarrow S_1$ hops, 50 $T_2 \rightarrow T_1$ hops, 36 $T_1 \rightarrow T_2$ hops (c). A net transfer is the difference between forward and backward hopping events.

3. Single Point Calculations of Geometries Along the Potential Energy Surface

The CASSCF(12,11) benchmark on Franck–Condon and S_1 minimum geometries was performed for different basis sets (Table S3), with the goal of reproducing with the lesser computational expenses the correct order of singlet and triplet states along the BP MEP studied at the single state (SS-)CASPT2(12,11)/ANO-L-VDZP level of theory (Sergentu, D.-C.; Maurice, R.; Havenith, R. W. A.; Broer, R.; Roca-Sanjuán, D. Computational Determination of the Dominant Triplet Population Mechanism in Photoexcited Benzophenone. *Phys. Chem. Chem. Phys.* **2014**, *16*, 25393–25403.), while being computationally feasible for dynamics.

Table S3. CASSCF(12,11) benchmark for benzophenone (Franck–Condon and S_1 minimum geometries) in gas phase.

Electronic state	Franck–Condon		S_1 minimum	
	Relative energy (kcal/mol)	SS-CASPT2 (kcal/mol)	Relative energy (kcal/mol)	SS-CASPT2 (kcal/mol)
	CASSCF(12,11)/6-31G*			
S_0	0	0	0	0
S_1	97.49	83.94	50.09	72.64
S_2	139.04	107.69	114.17	
T_1	87.99	71.72	46.65	64.57
T_2	98.46	82.32	57.11	80.71
T_3	98.78	83.00	88.10	89.93
	CASSCF(12,11)/ANO-S-VDZP			
S_0	0	0	0	0
S_1	111.33	83.94	48.62	72.64
S_2	129.60	107.69	111.61	
T_1	84.92	71.72	45.56	64.57
T_2	95.59	82.32	55.79	80.71
T_3	110.65	83.00	86.25	89.93
	CASSCF(12,11)/ANO-L-VDZP			
S_0	0	0	0	0
S_1	97.20	83.94	48.52	72.64
S_2	112.16	107.69	111.54	
T_1	85.89	71.72	45.48	64.57
T_2	95.80	82.32	55.72	80.71
T_3	111.66	83.00	86.31	89.93
	CASSCF(12,11)/ANO-RCC-VQZP			
S_0	0	0	0	0
S_1	87.48	83.94	46.14	72.64
S_2	148.17	107.69	114.65	
T_1	79.08	71.72	41.24	64.57
T_2	99.01	82.32	56.61	80.71
T_3	104.68	83.00	93.50	89.93

The values reported in Table S4 refer to benzophenone in water solvent, taken into account by a polarizable continuum model (PCM) through state averaged calculations at the CASSCF level.

Table S4. CASSCF(12,11) energy values for benzophenone (Franck–Condon geometry) in water solvent (PCM method).

Electronic state	Relative energy (kcal/mol)
	CASSCF(12,11)/ANO-S-VDZP
S_0	0
S_1	111.33
S_2	129.06
T_1	83.40
T_2	108.02
T_3	109.24
	CASSCF(12,11)/ANO-L-VDZP
S_0	0
S_1	112.65
S_2	129.21
T_1	84.47
T_2	108.93
T_3	110.64

Figure S3 shows the agreement between CASSCF(12,11)/ANO-S-VDZP and SS-CASPT2(12,11)/ANO-L-VDZP along the excited state MEP. As can be seen S_1, T_2 and T_1 energies are close (interval of 0.35 eV) at the T_1 minimum geometry.

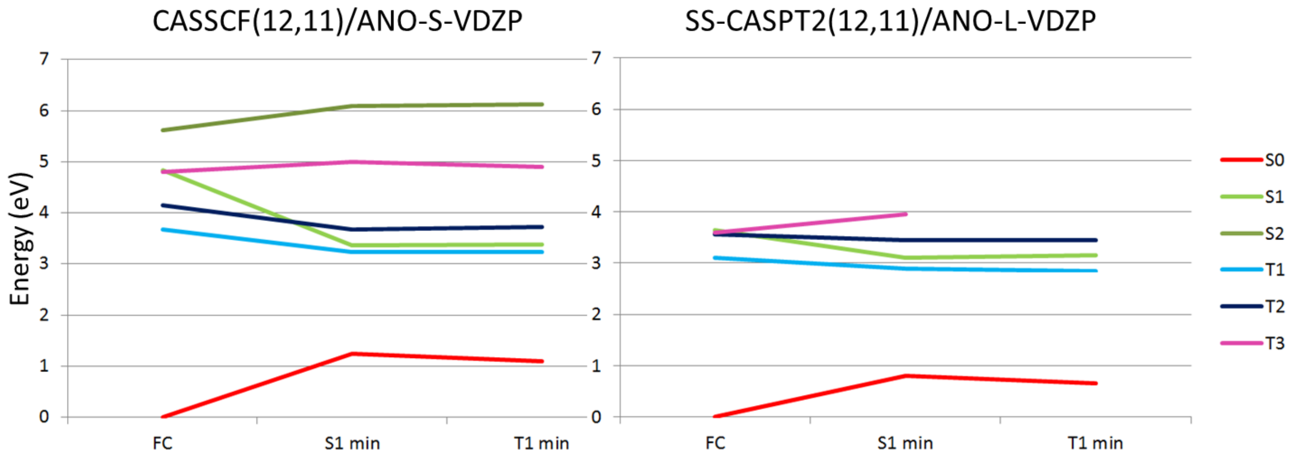

Figure S3. Comparison between CASSCF and CASPT2 energetics along the MEP. The CASPT2 results are taken from Sergentu at al. *Phys. Chem. Chem. Phys.* **2014**, *16*, 25393–25403.

We note that the CASPT2 level of theory is more accurate than the CASSCF level of theory. Nevertheless, presently CASPT2 dynamics are not feasible, since the present implementations of the CASPT2 analytical energy gradient are impractical for molecules of the size of BP. The same can be said about the use of the CASPT2 numerical energy gradient.

4. Wavefunction Amplitude Graphs of the 39 Trajectories Populating the Triplet manifold

The following graphs show the wavefunction amplitude as a function of the time (fs), for all 39 trajectories where a successful population of the triplet manifold was observed. All electronic states considered for the simulation (the singlets S_0, S_1, S_2 and the triplets T_1, T_2, T_3) are shown. The wavefunction amplitude is calculated as the sum of the absolute squares of the MCH (molecular Coulomb Hamiltonian) coefficients for each state. For triplets, multiplet components are summed up. Most of the trajectories were stopped when the sum of the wavefunction amplitudes of a certain triplet state – including multiple components – equal to one; while 15 trajectories were calculated for additional time, in order to study the kinetic equilibrium between triplet states, and check the eventuality of re-crossing to populate back the singlet state (observed only once).

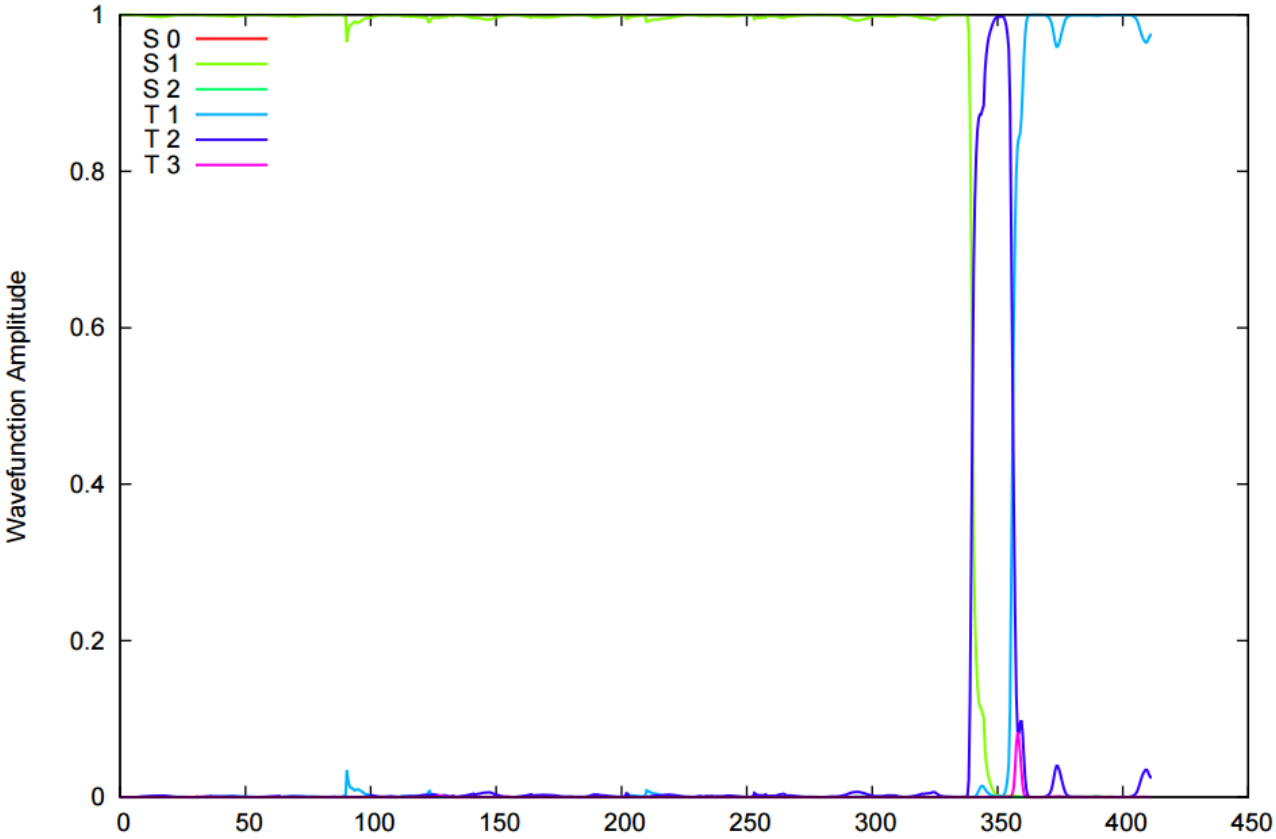

Wavefunction Amplitude
S 0
S 1
S 2
T 1
T 2
T 3
0
0.2
0.4
0.6
0.8
1
0
50
100
150
200
250
300
350
400
450

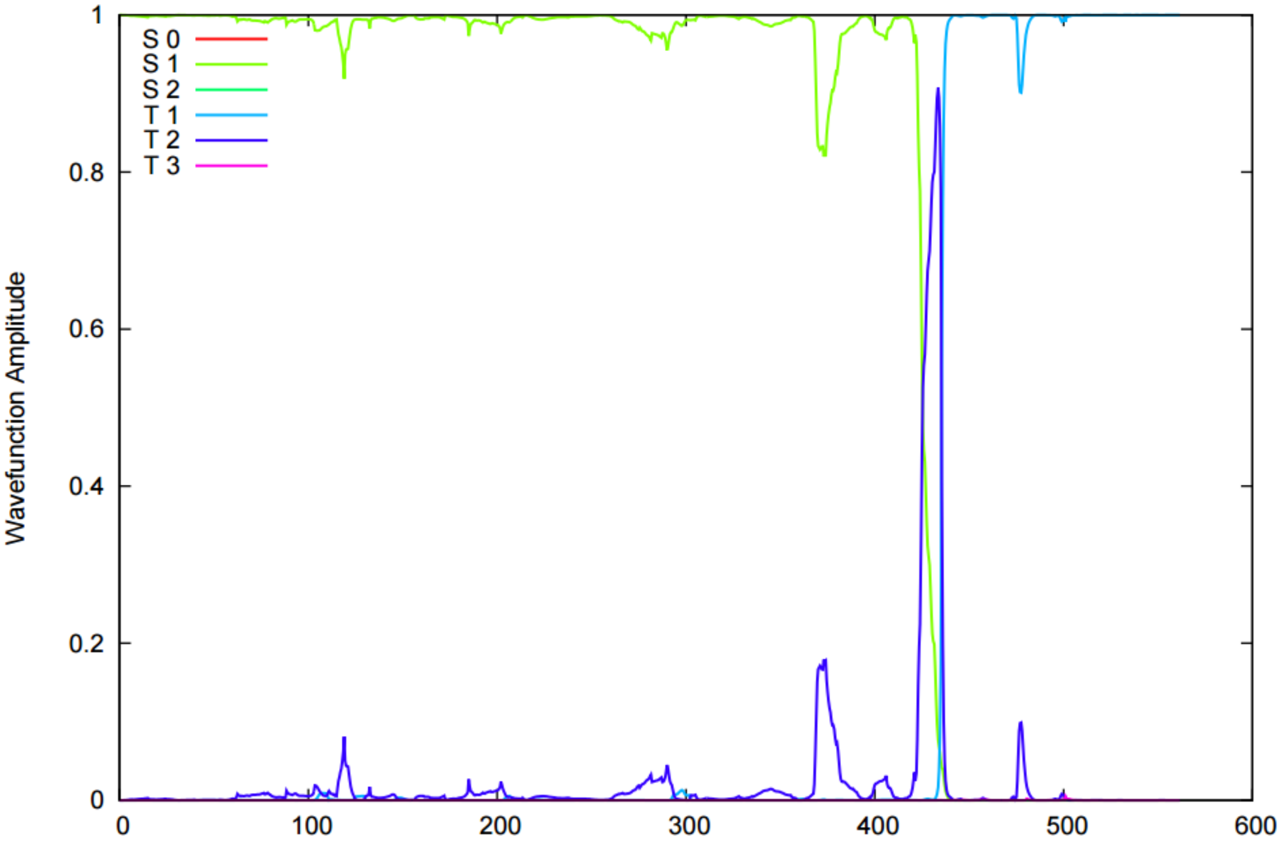

Wavefunction Amplitude
S 0
S 1
S 2
T 1
T 2
T 3
0
0.2
0.4
0.6
0.8
1
0
100
200
300
400
500
600

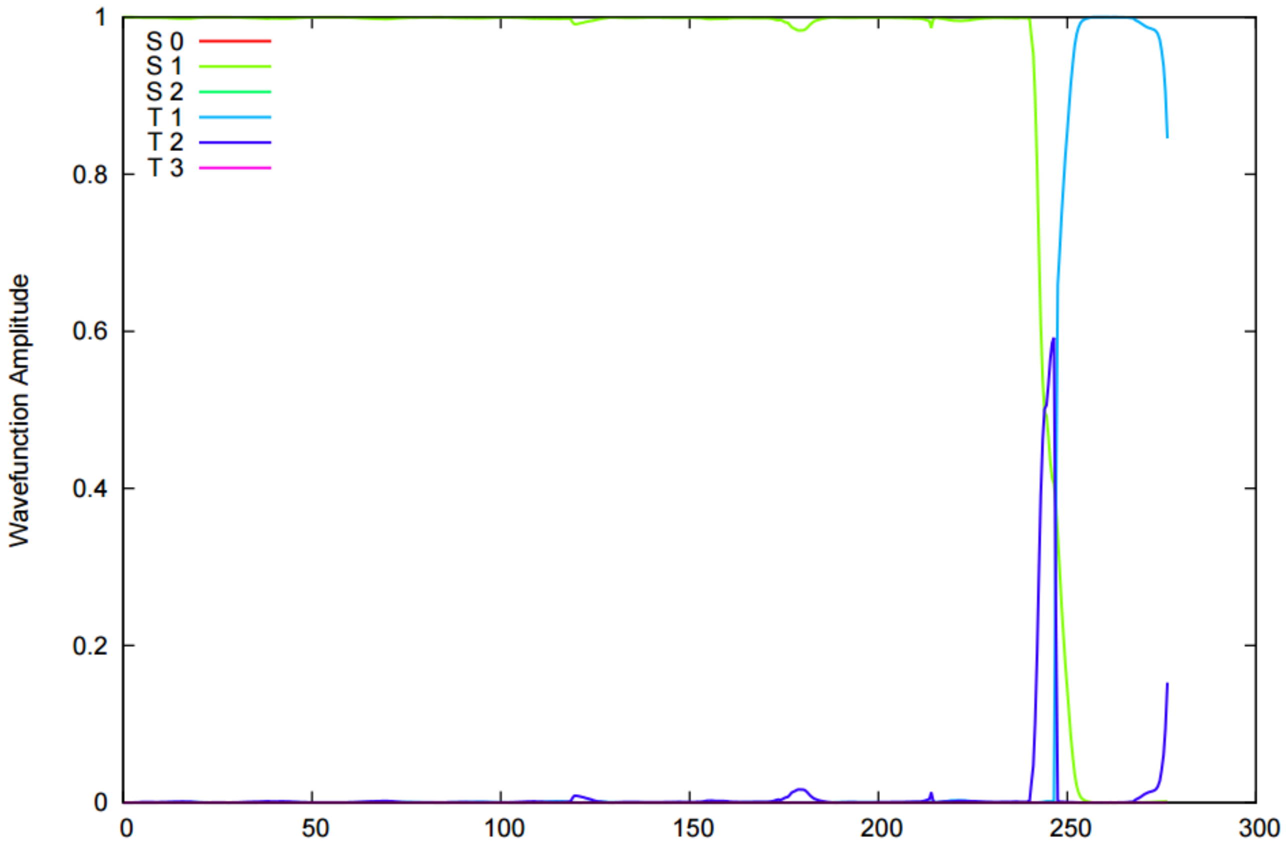
Wavefunction Amplitude
S 0
S 1
S 2
T 1
T 2
T 3
1
0.8
0.6
0.4
0.2
0
0
50
100
150
200
250
300

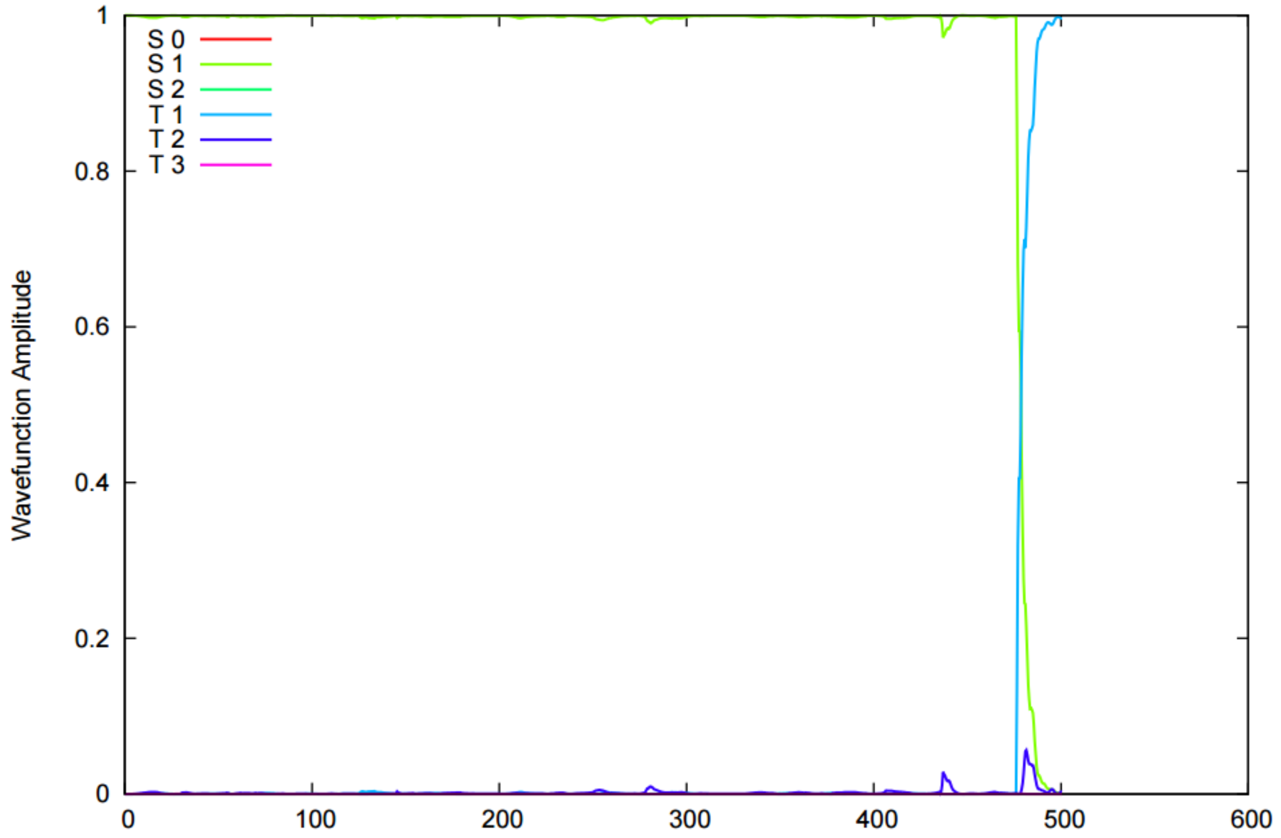
Wavefunction Amplitude
S 0
S 1
S 2
T 1
T 2
T 3
1
0.8
0.6
0.4
0.2
0
0
100
200
300
400
500
600

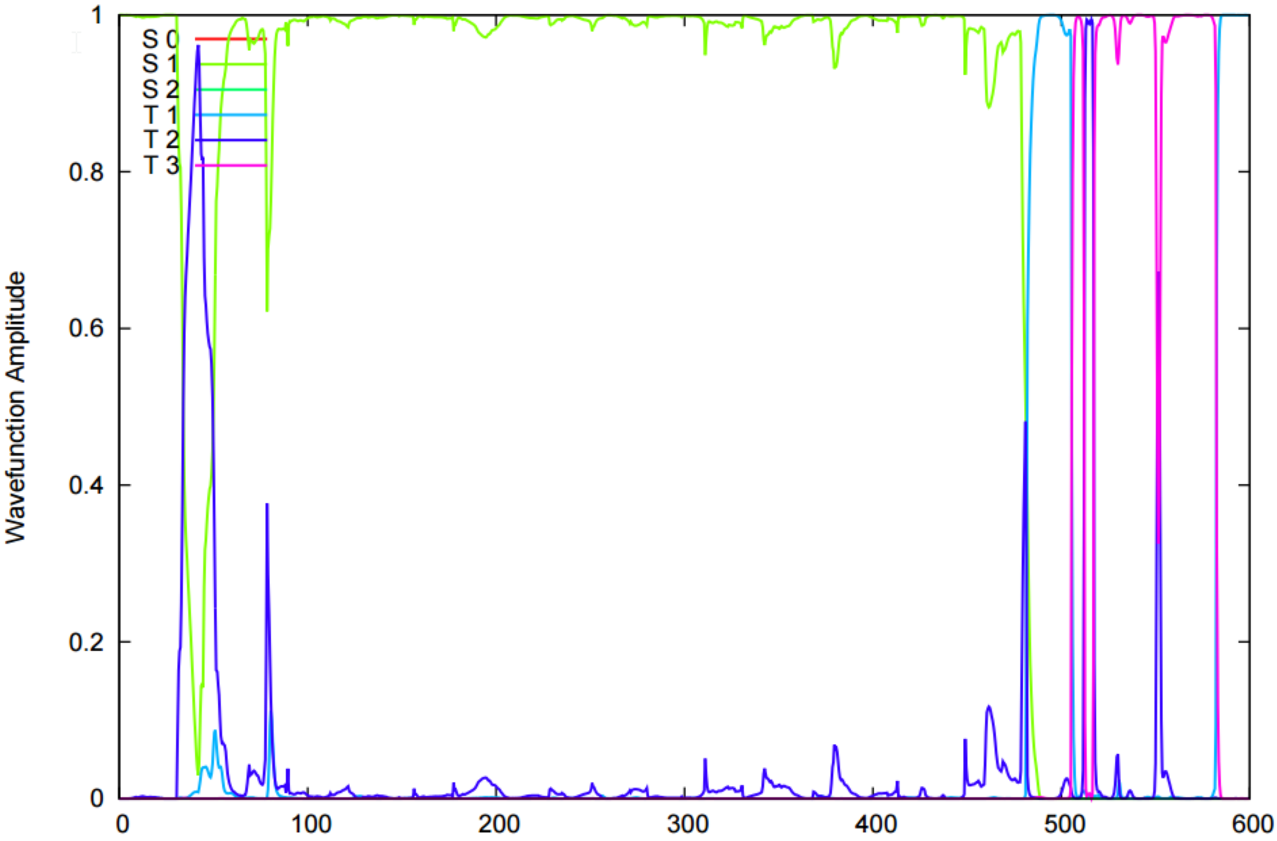
Wavefunction Amplitude
S 0
S 1
S 2
T 1
T 2
T 3
0
0.2
0.4
0.6
0.8
1
0
100
200
300
400
500
600

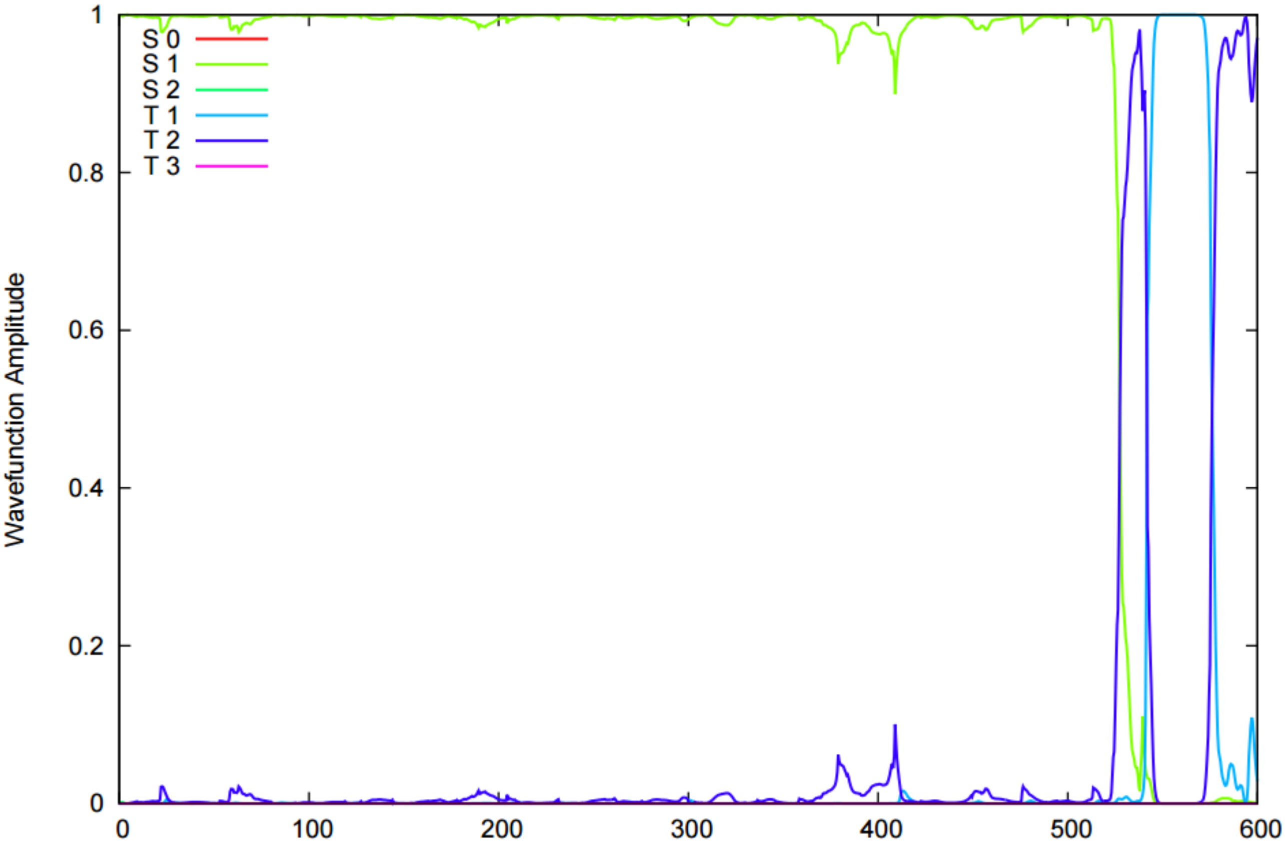
Wavefunction Amplitude
S 0
S 1
S 2
T 1
T 2
T 3
0
0.2
0.4
0.6
0.8
1
0
100
200
300
400
500
600

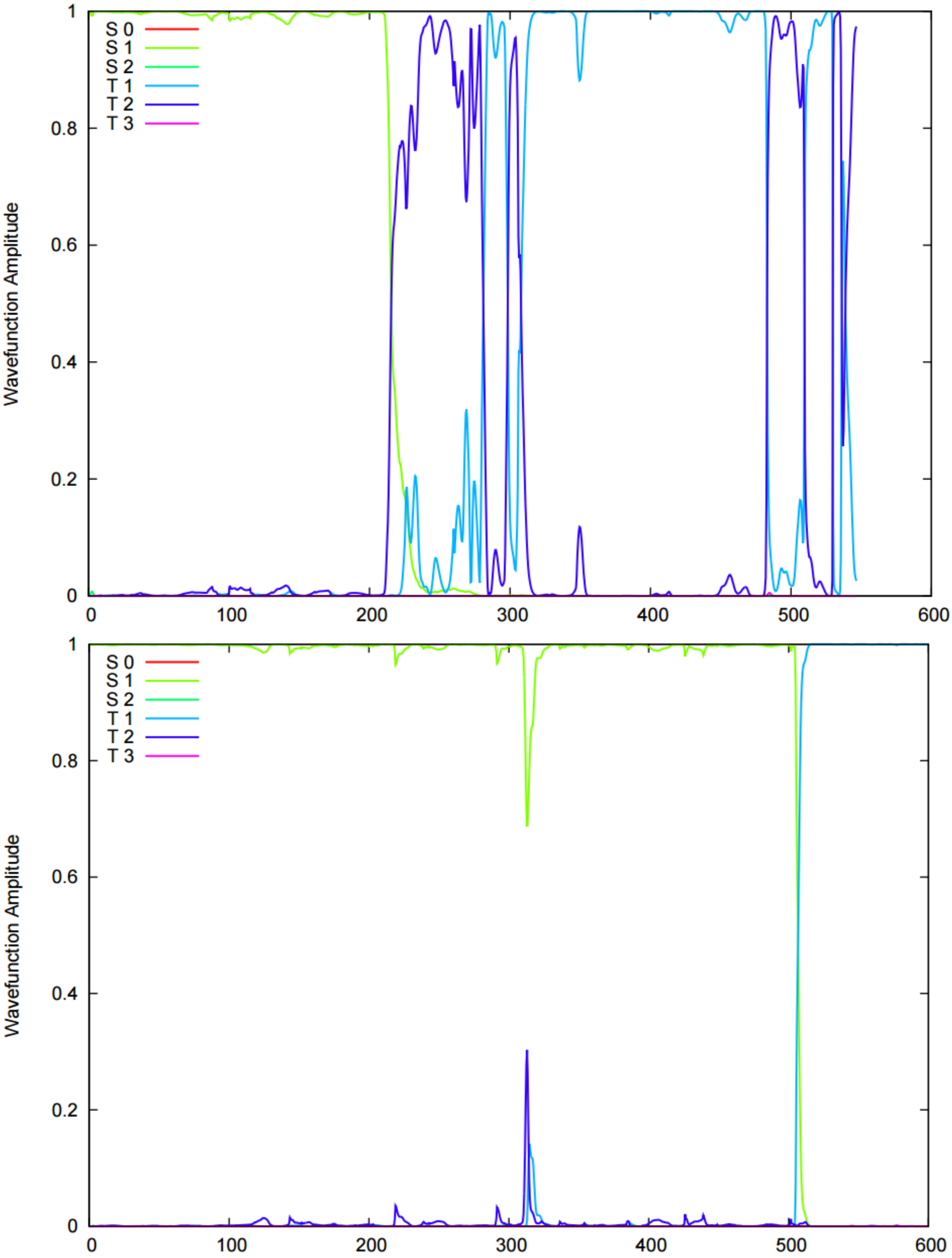
Wavefunction Amplitude
S 0
S 1
S 2
T 1
T 2
T 3
0
0.2
0.4
0.6
0.8
1
0
100
200
300
400
500
600
Wavefunction Amplitude
S 0
S 1
S 2
T 1
T 2
T 3
0
0.2
0.4
0.6
0.8
1
0
100
200
300
400
500
600

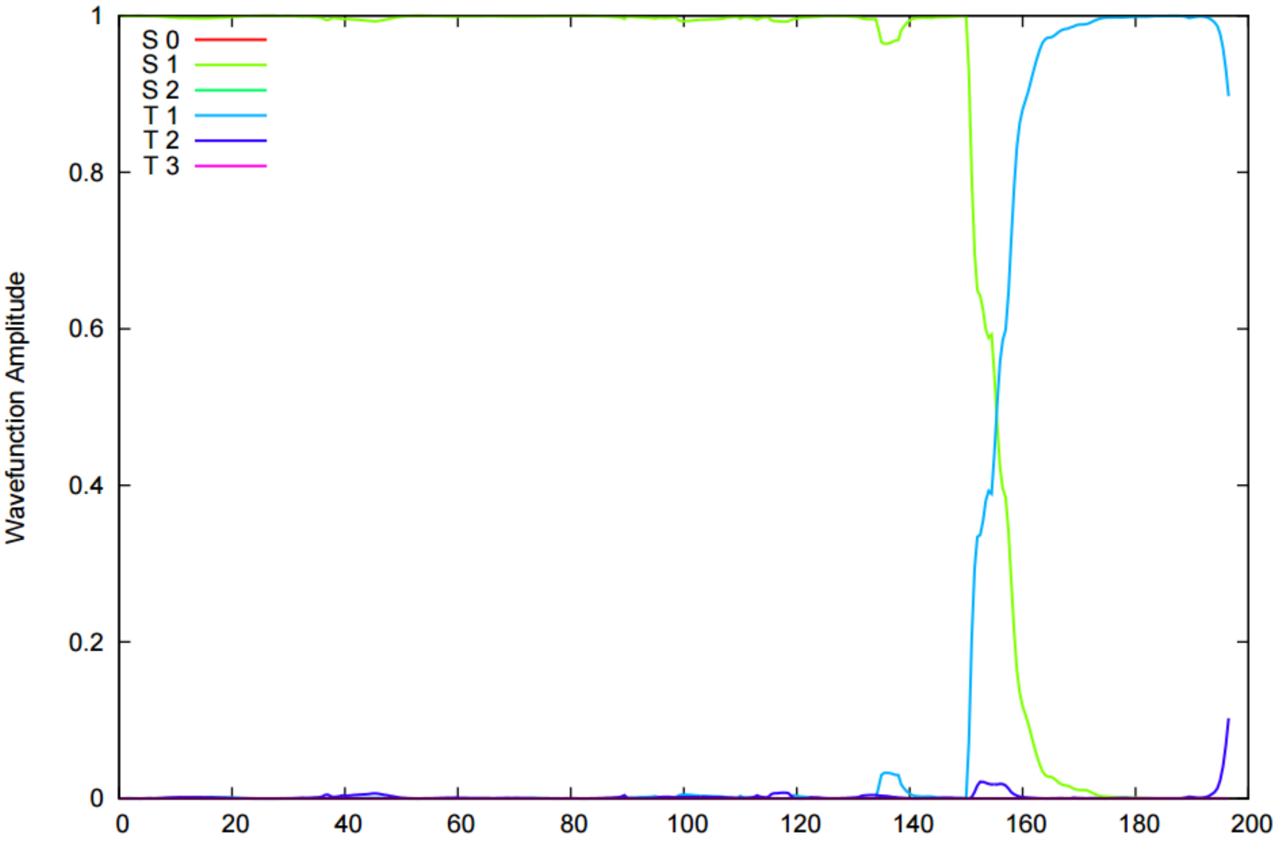
S 0
S 1
S 2
T 1
T 2
T 3
Wavefunction Amplitude
0
0.2
0.4
0.6
0.8
1
0
20
40
60
80
100
120
140
160
180
200

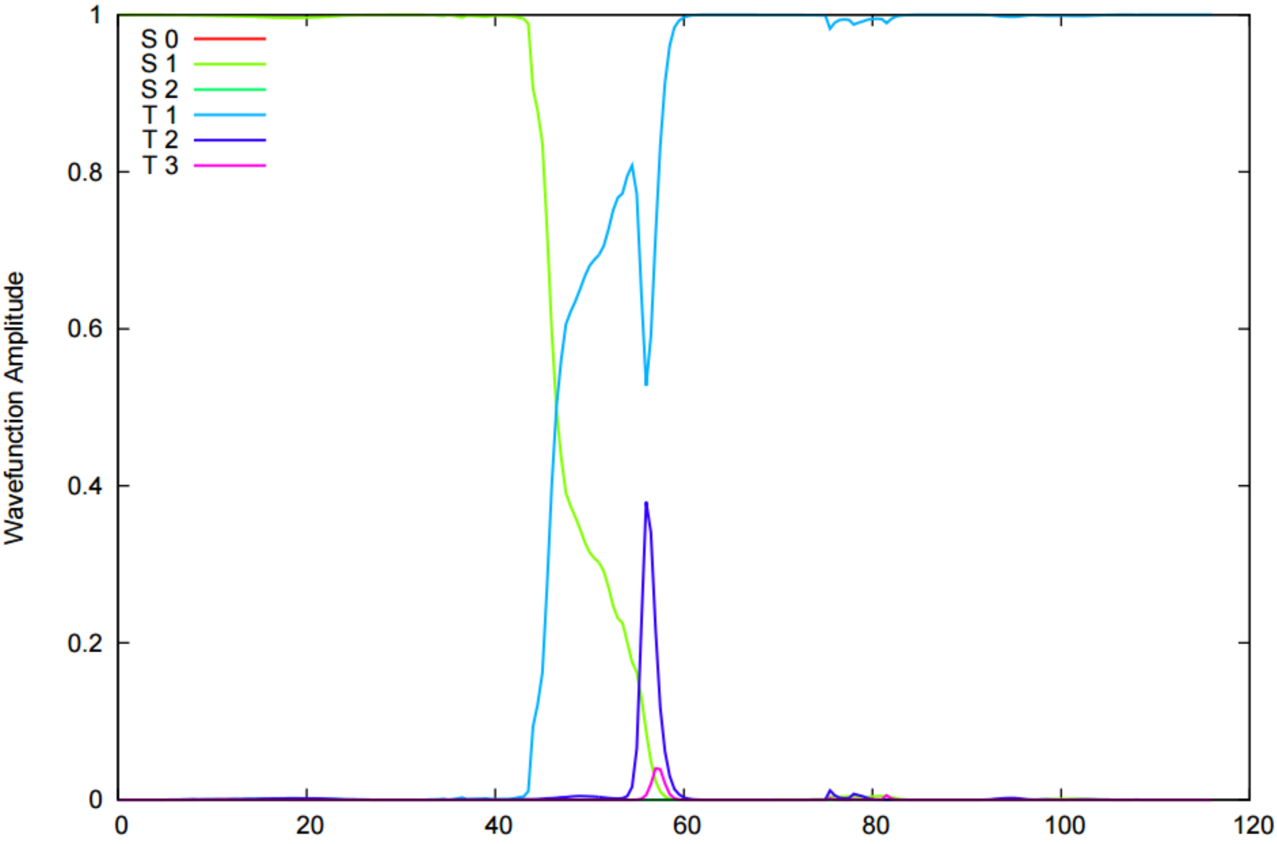
S 0
S 1
S 2
T 1
T 2
T 3
Wavefunction Amplitude
0
0.2
0.4
0.6
0.8
1
0
20
40
60
80
100
120

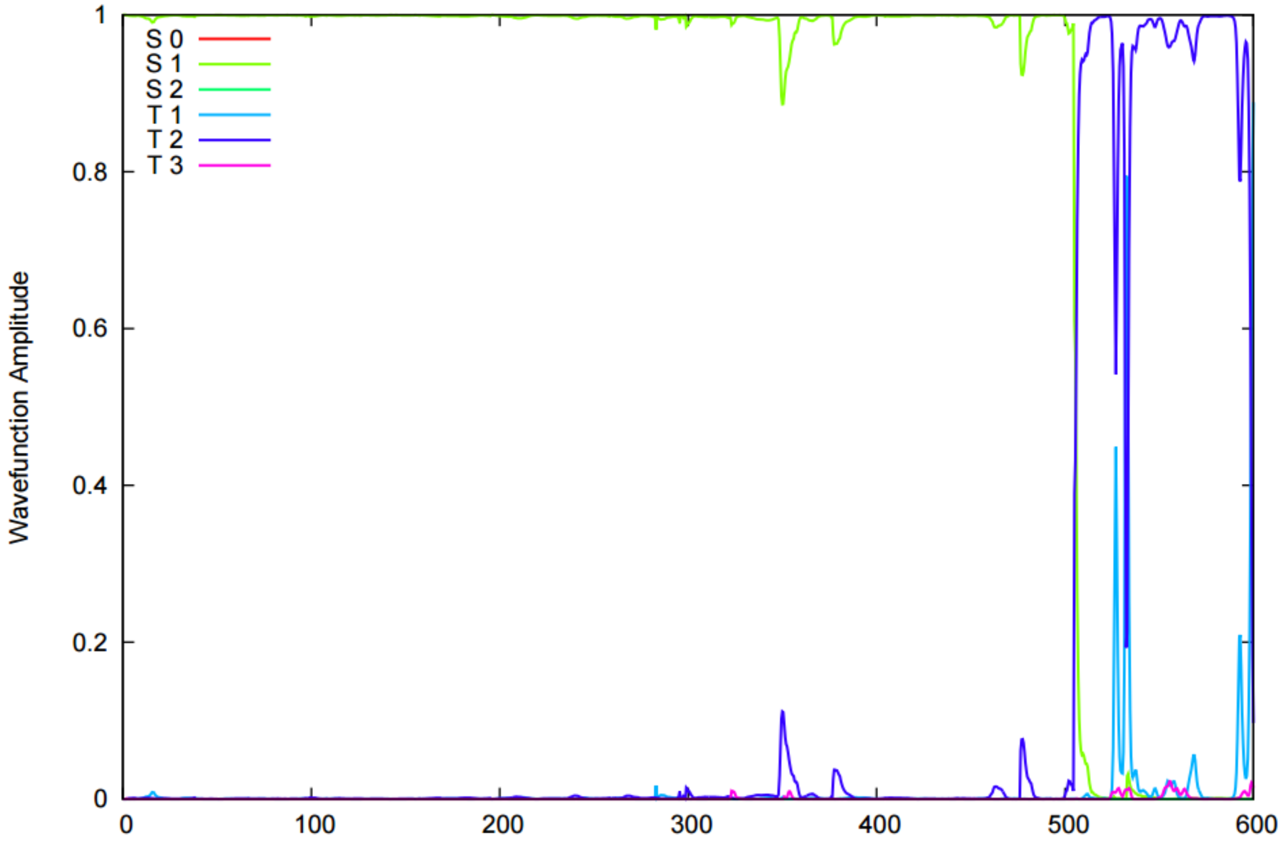
Wavefunction Amplitude
S 0
S 1
S 2
T 1
T 2
T 3
0
0.2
0.4
0.6
0.8
1
0
100
200
300
400
500
600

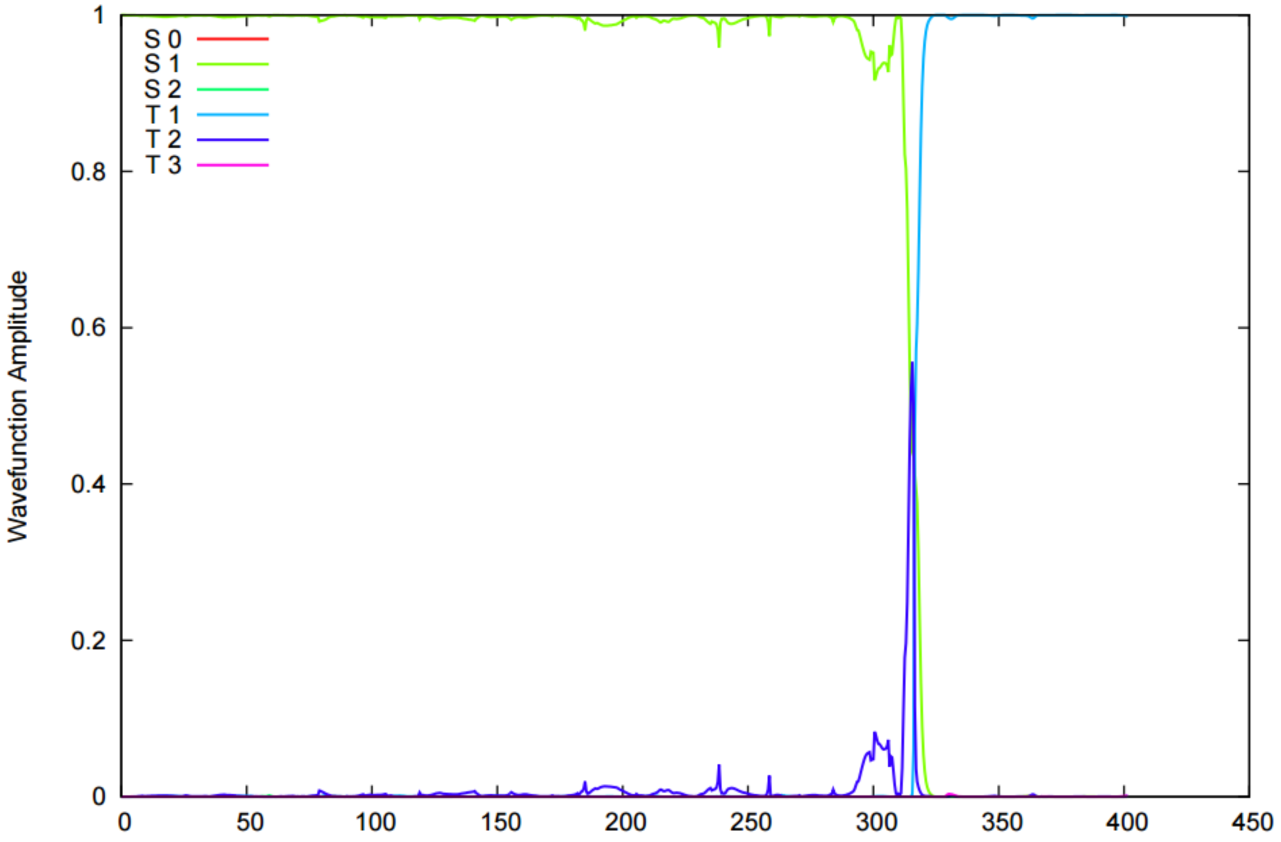
Wavefunction Amplitude
S 0
S 1
S 2
T 1
T 2
T 3
0
0.2
0.4
0.6
0.8
1
0
50
100
150
200
250
300
350
400
450

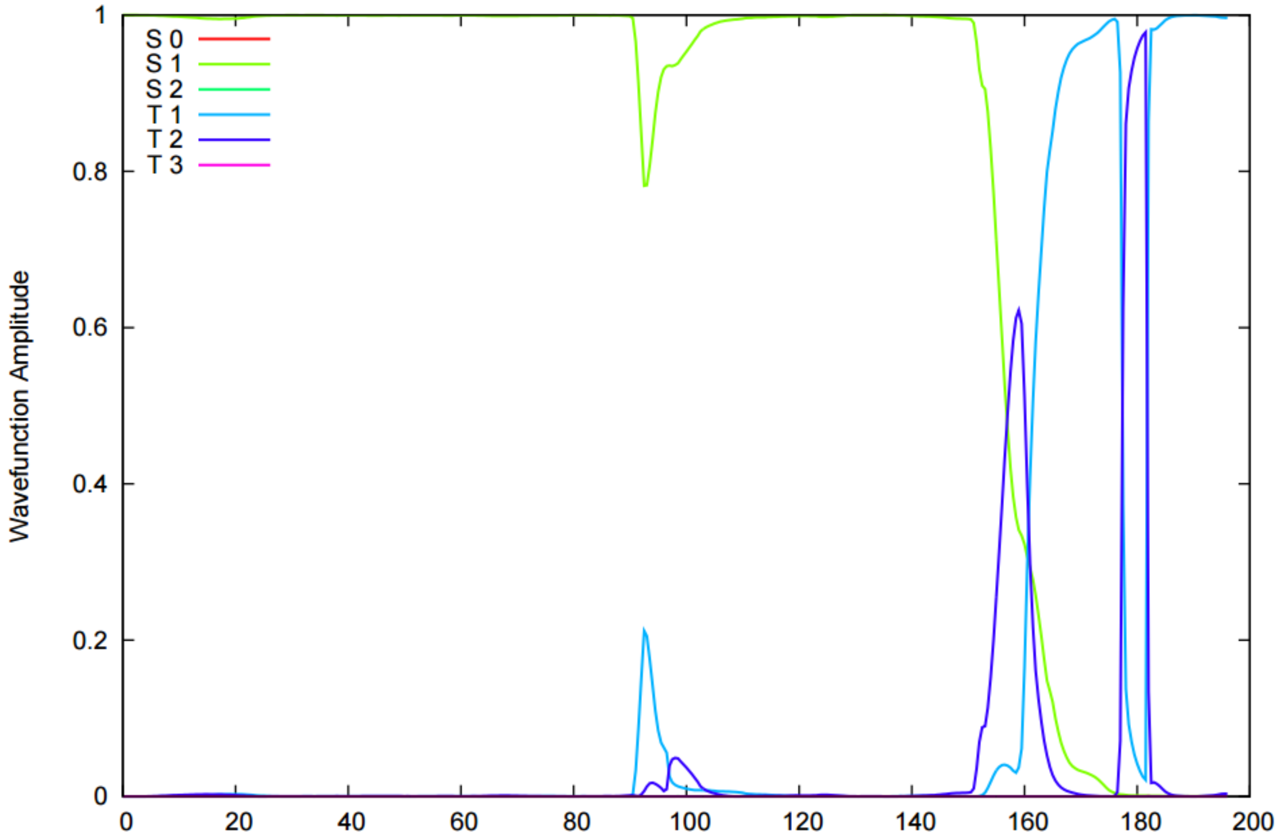
Wavefunction Amplitude
S 0
S 1
S 2
T 1
T 2
T 3
1
0.8
0.6
0.4
0.2
0
0
20
40
60
80
100
120
140
160
180
200

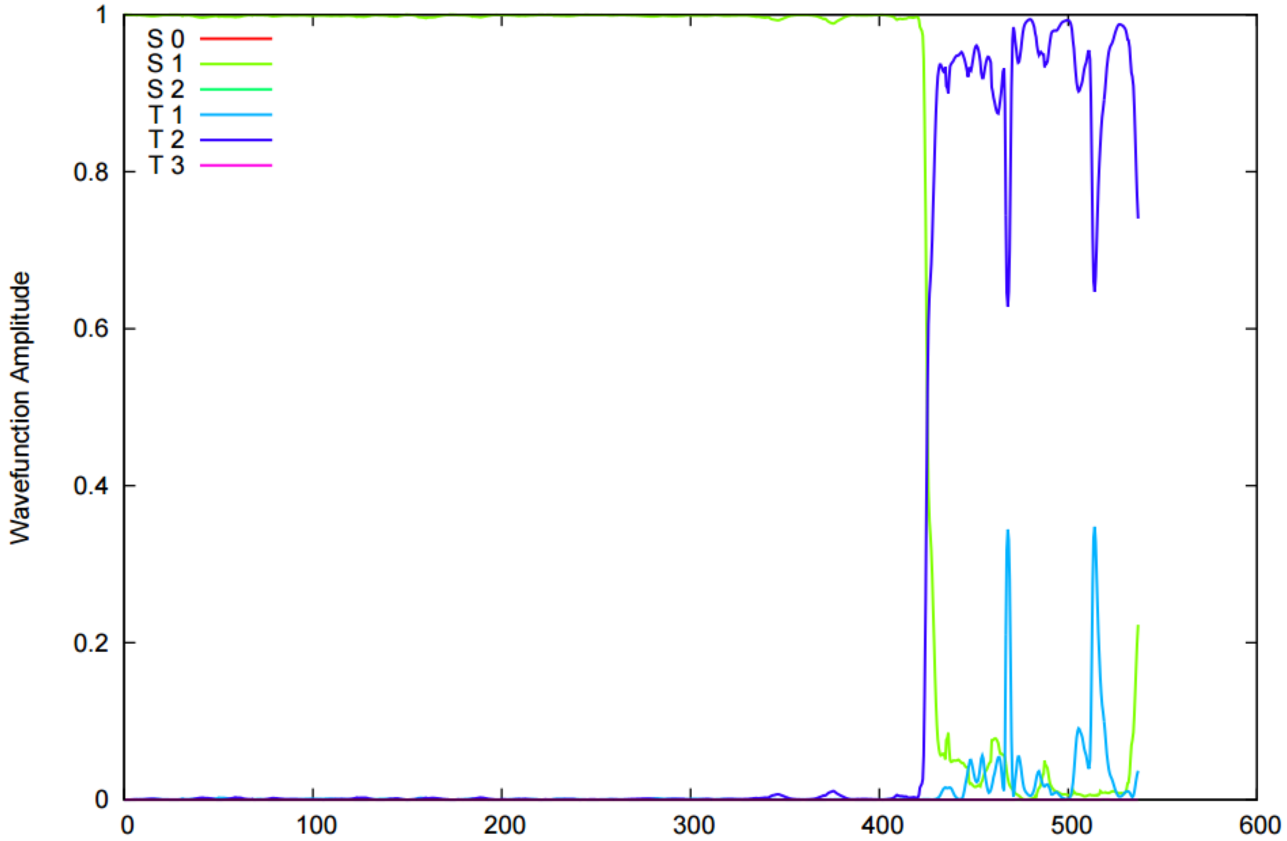
Wavefunction Amplitude
S 0
S 1
S 2
T 1
T 2
T 3
1
0.8
0.6
0.4
0.2
0
0
100
200
300
400
500
600

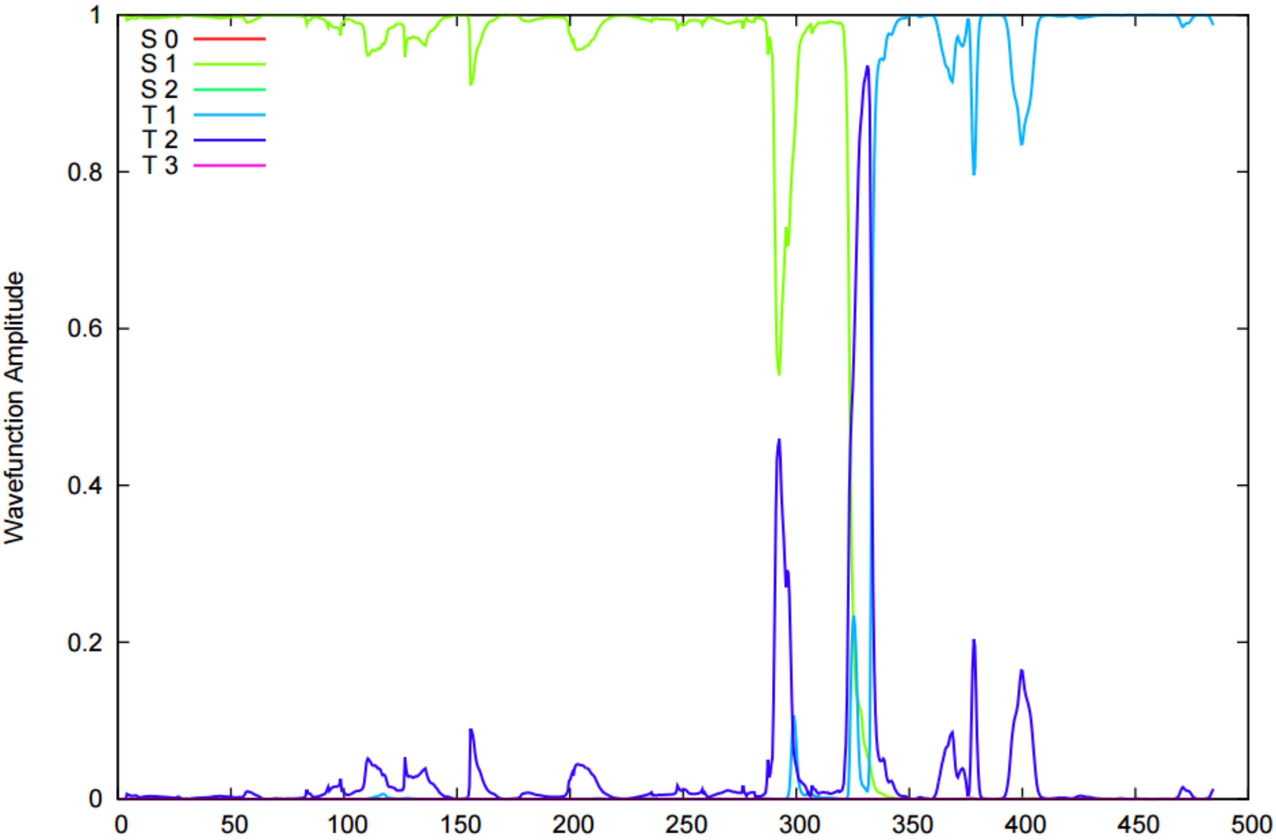
Wavefunction Amplitude
S 0
S 1
S 2
T 1
T 2
T 3
0
0.2
0.4
0.6
0.8
1
0
50
100
150
200
250
300
350
400
450
500

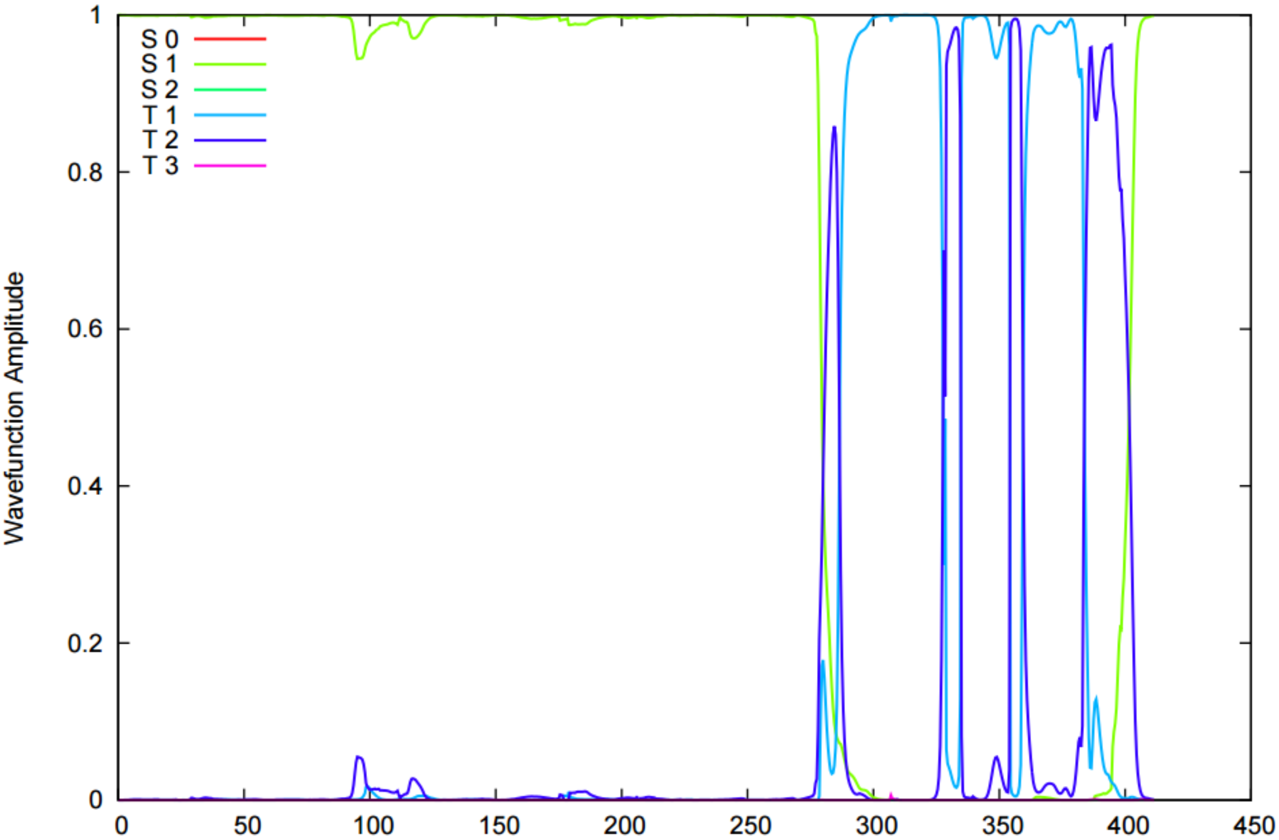
Wavefunction Amplitude
S 0
S 1
S 2
T 1
T 2
T 3
0
0.2
0.4
0.6
0.8
1
0
50
100
150
200
250
300
350
400
450

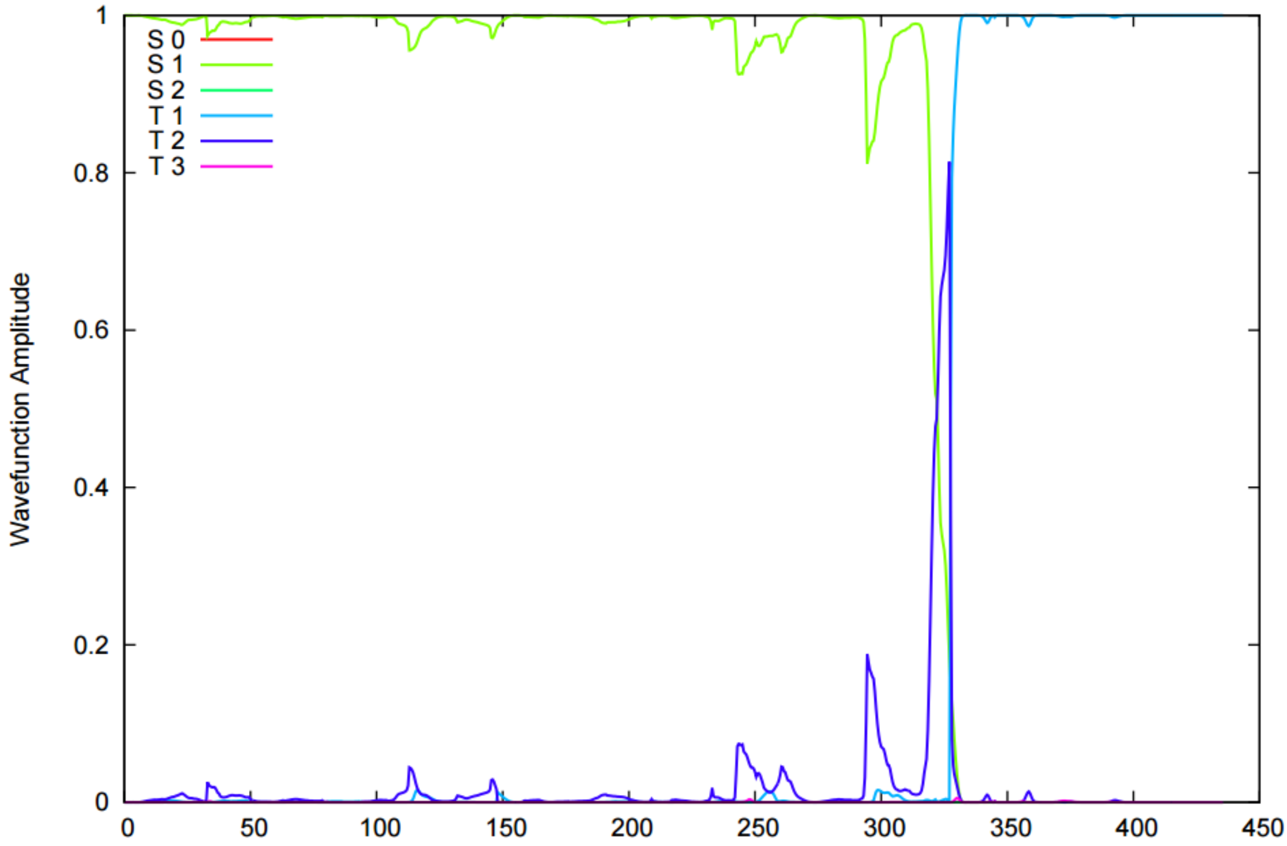
S 0
S 1
S 2
T 1
T 2
T 3
Wavefunction Amplitude
0
0.2
0.4
0.6
0.8
1
0
50
100
150
200
250
300
350
400
450

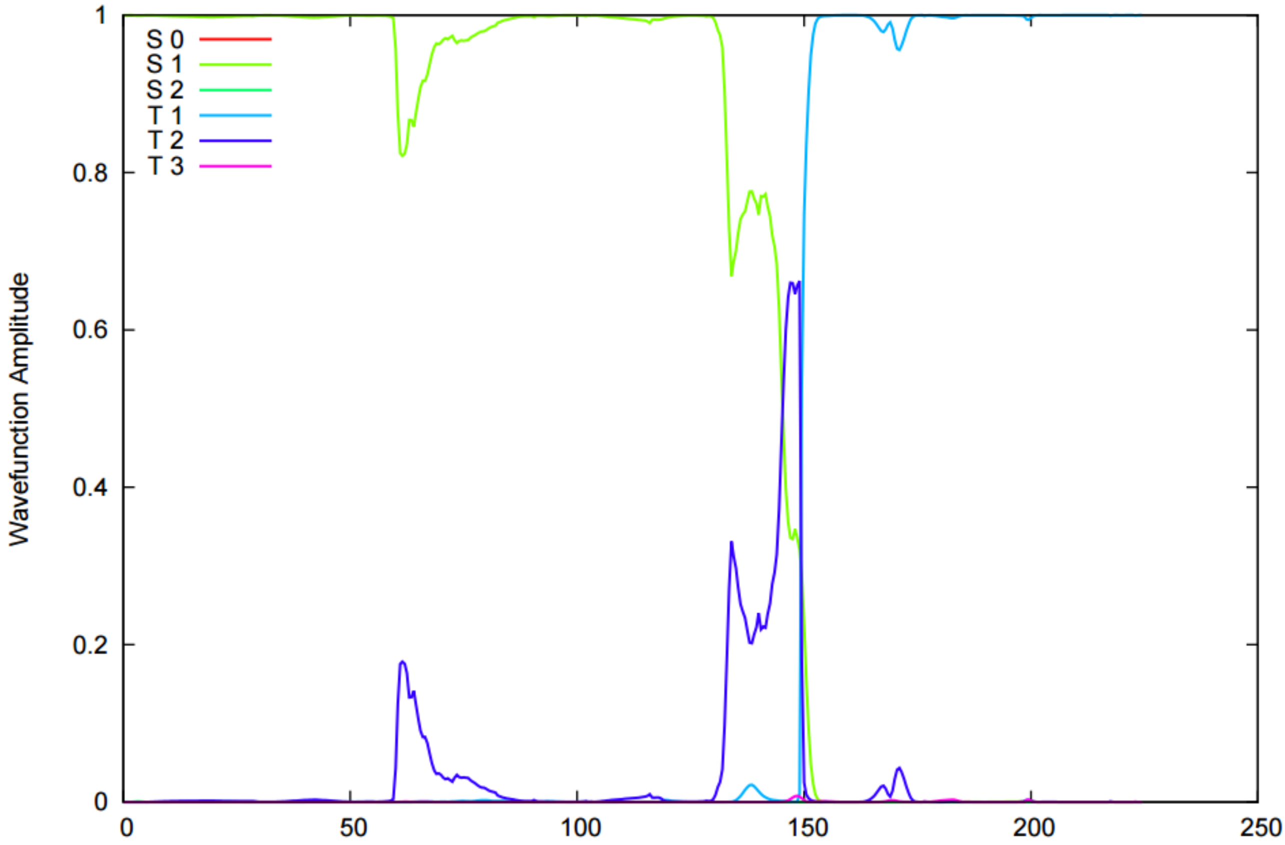
S 0
S 1
S 2
T 1
T 2
T 3
Wavefunction Amplitude
0
0.2
0.4
0.6
0.8
1
0
50
100
150
200
250

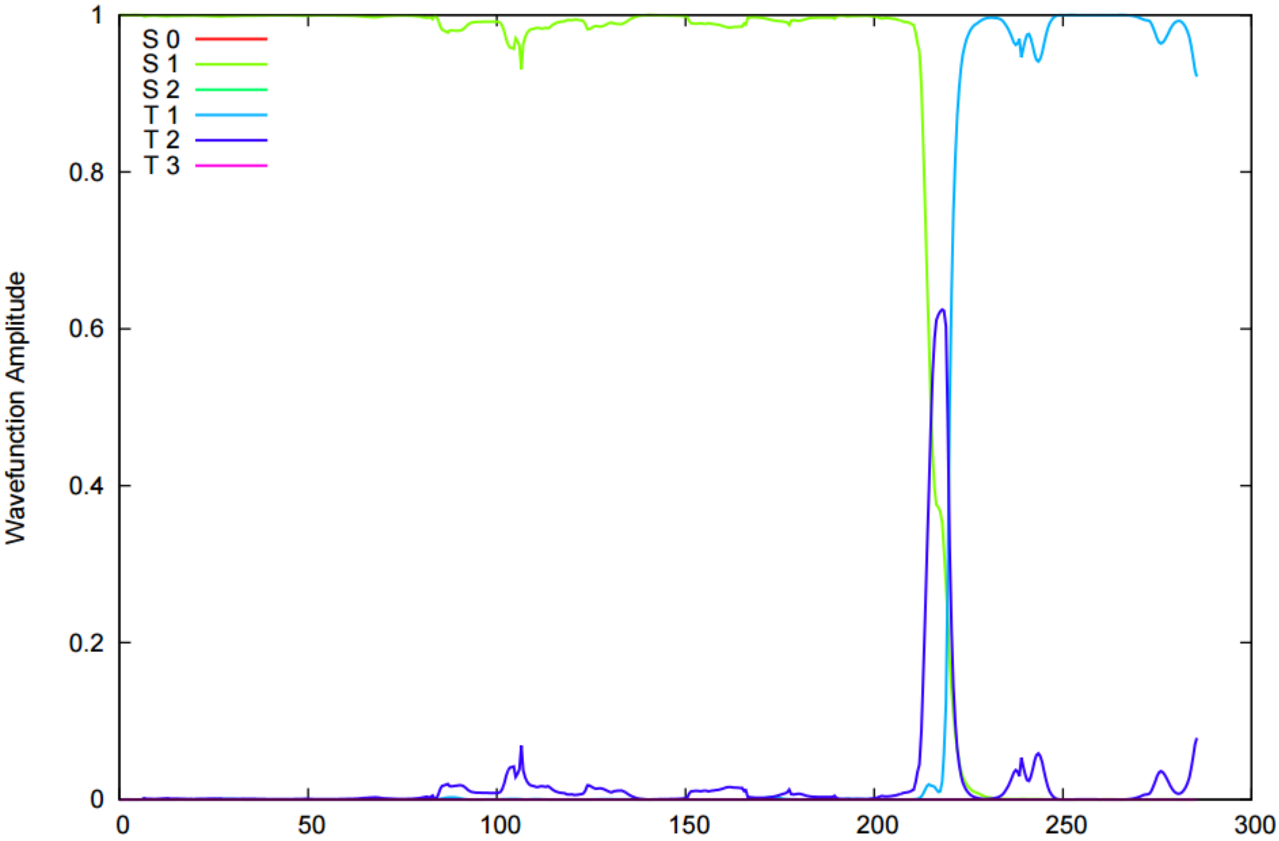
S 0
S 1
S 2
T 1
T 2
T 3
Wavefunction Amplitude
1
0.8
0.6
0.4
0.2
0
0
50
100
150
200
250
300

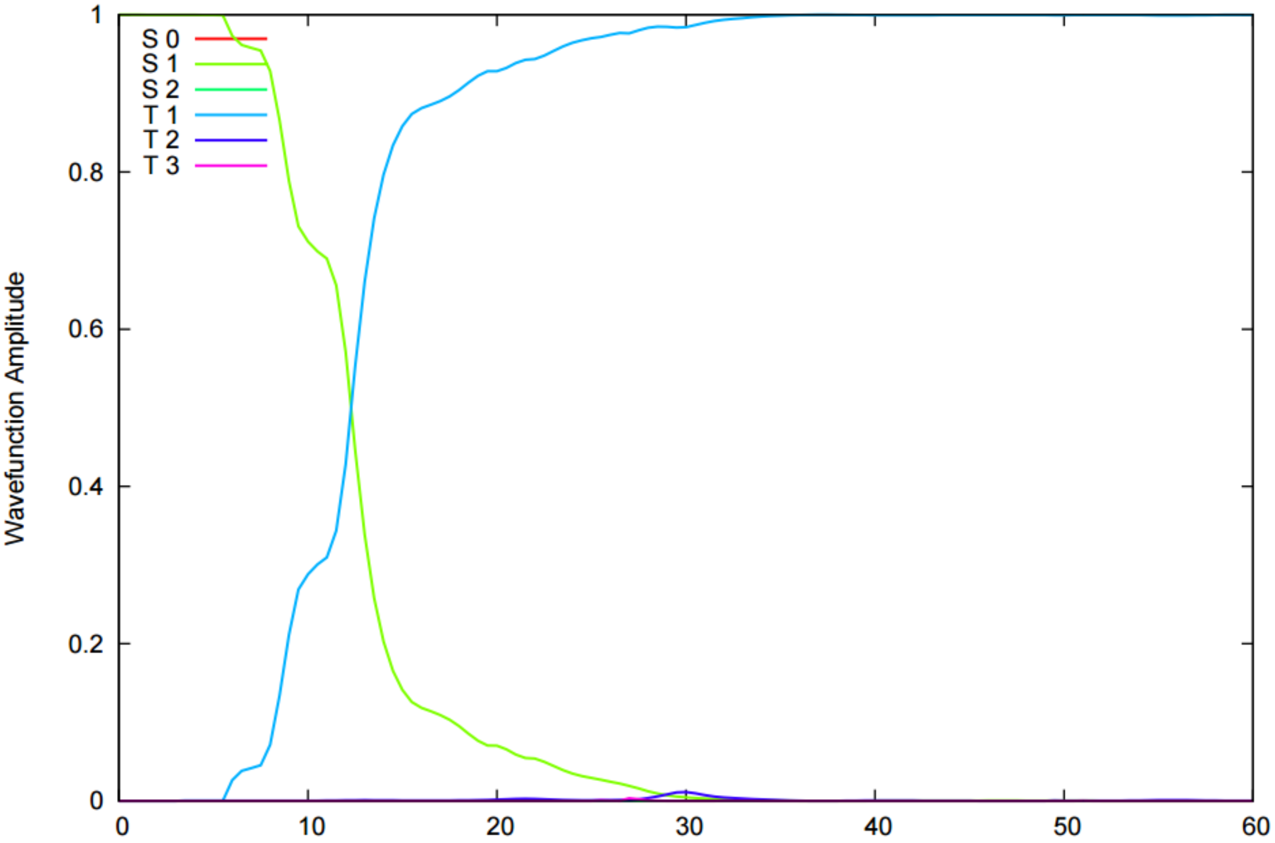
S 0
S 1
S 2
T 1
T 2
T 3
Wavefunction Amplitude
1
0.8
0.6
0.4
0.2
0
0
10
20
30
40
50
60

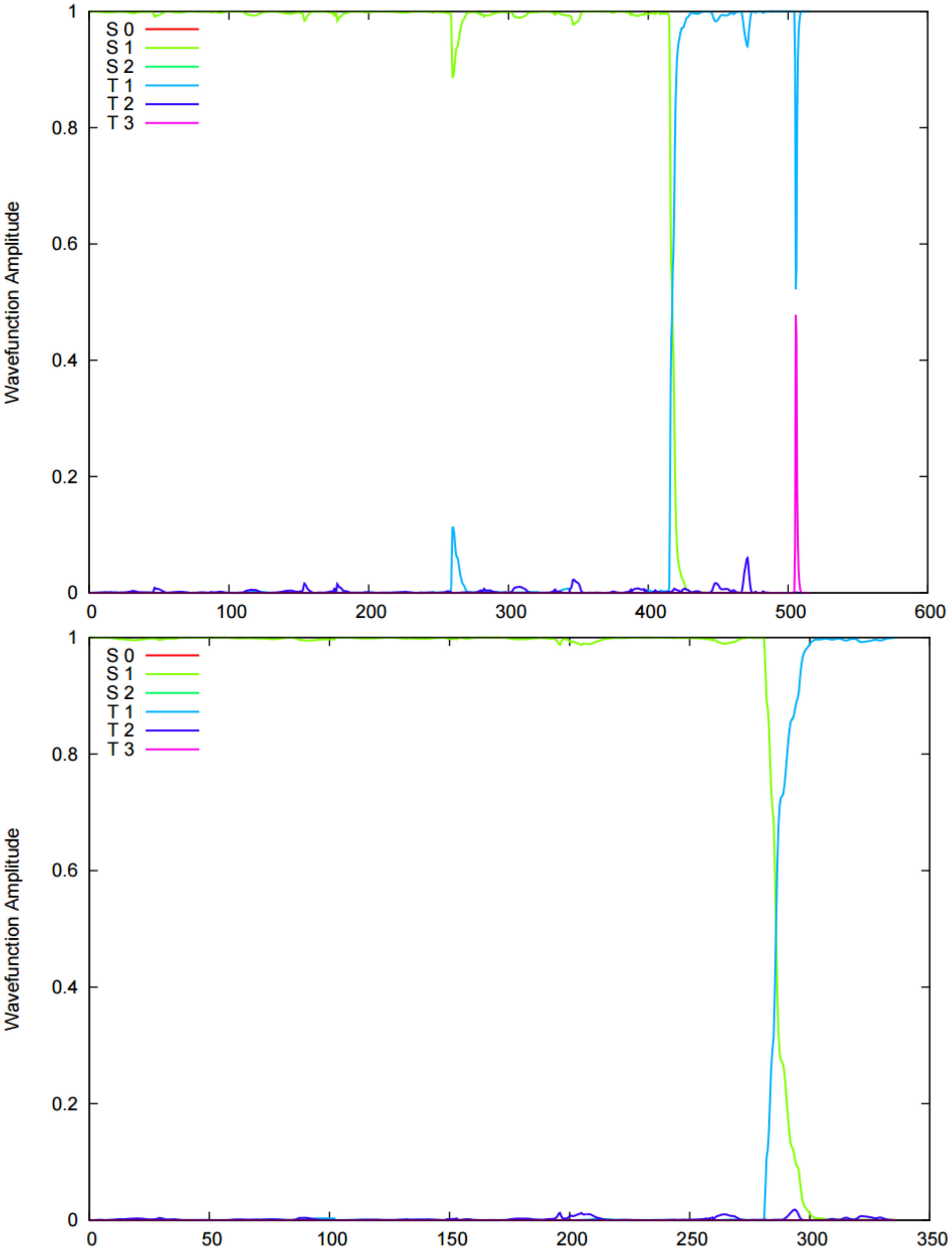
S 0
S 1
S 2
T 1
T 2
T 3
Wavefunction Amplitude
0
0.2
0.4
0.6
0.8
1
0
100
200
300
400
500
600
S 0
S 1
S 2
T 1
T 2
T 3
Wavefunction Amplitude
0
0.2
0.4
0.6
0.8
1
0
50
100
150
200
250
300
350

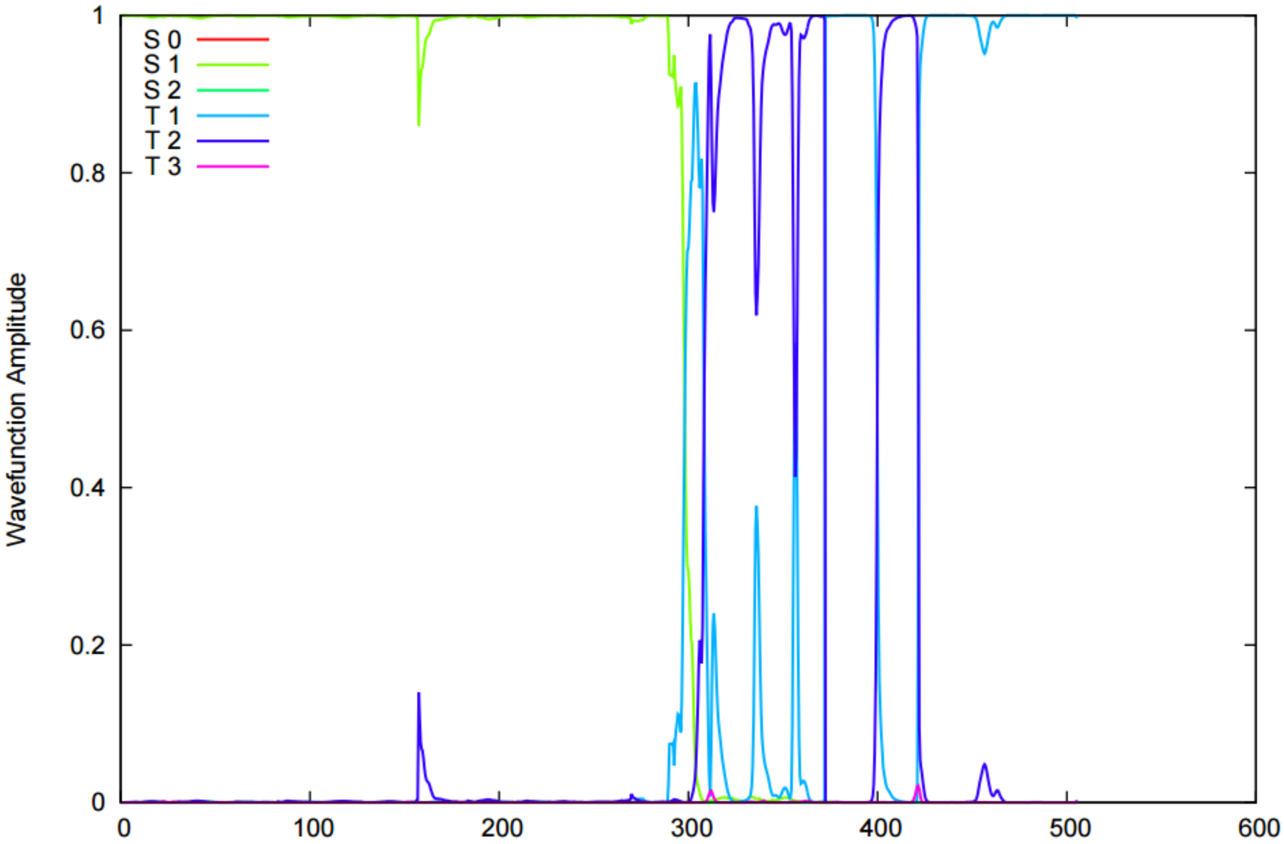
S 0
S 1
S 2
T 1
T 2
T 3
Wavefunction Amplitude
0
0.2
0.4
0.6
0.8
1
0
100
200
300
400
500
600

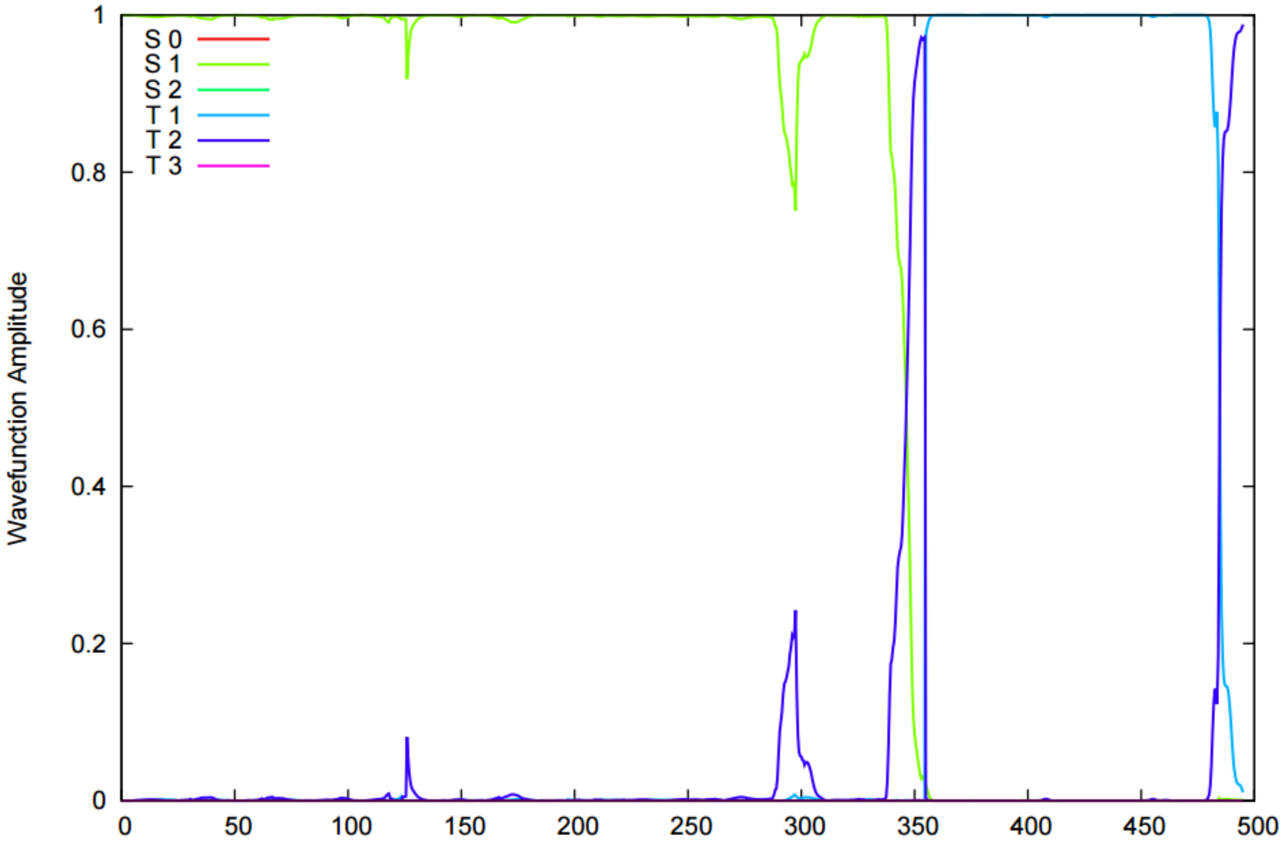
S 0
S 1
S 2
T 1
T 2
T 3
Wavefunction Amplitude
0
0.2
0.4
0.6
0.8
1
0
50
100
150
200
250
300
350
400
450
500

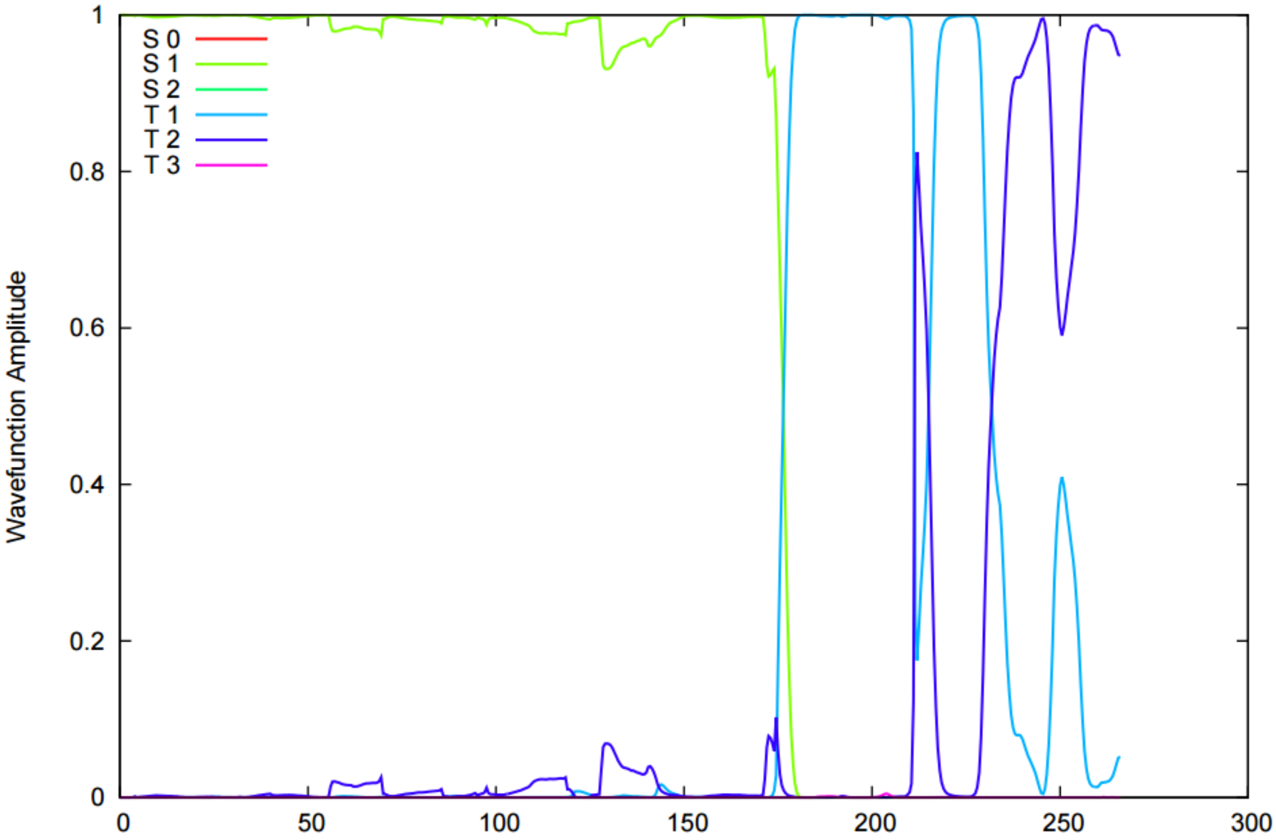
Wavefunction Amplitude
S 0
S 1
S 2
T 1
T 2
T 3
0
0.2
0.4
0.6
0.8
1
0
50
100
150
200
250
300

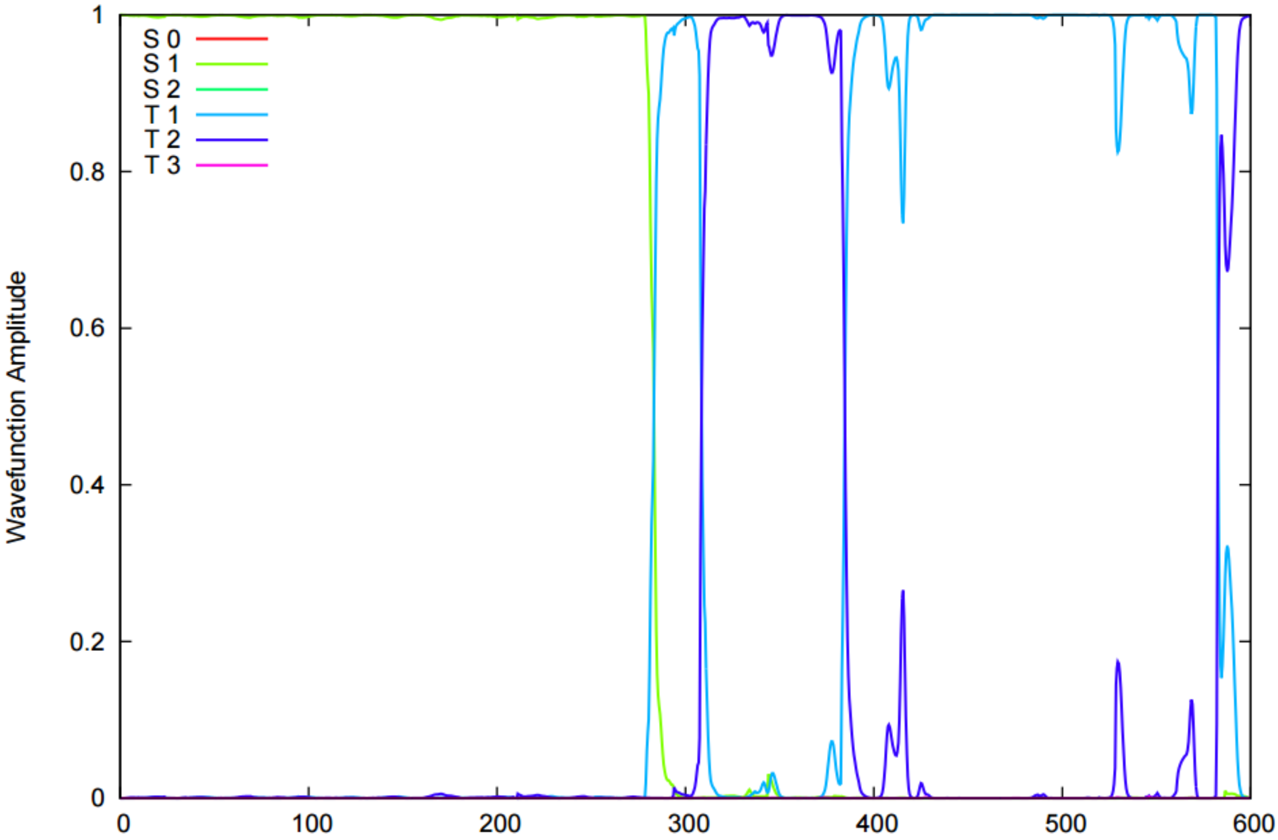
Wavefunction Amplitude
S 0
S 1
S 2
T 1
T 2
T 3
0
0.2
0.4
0.6
0.8
1
0
100
200
300
400
500
600

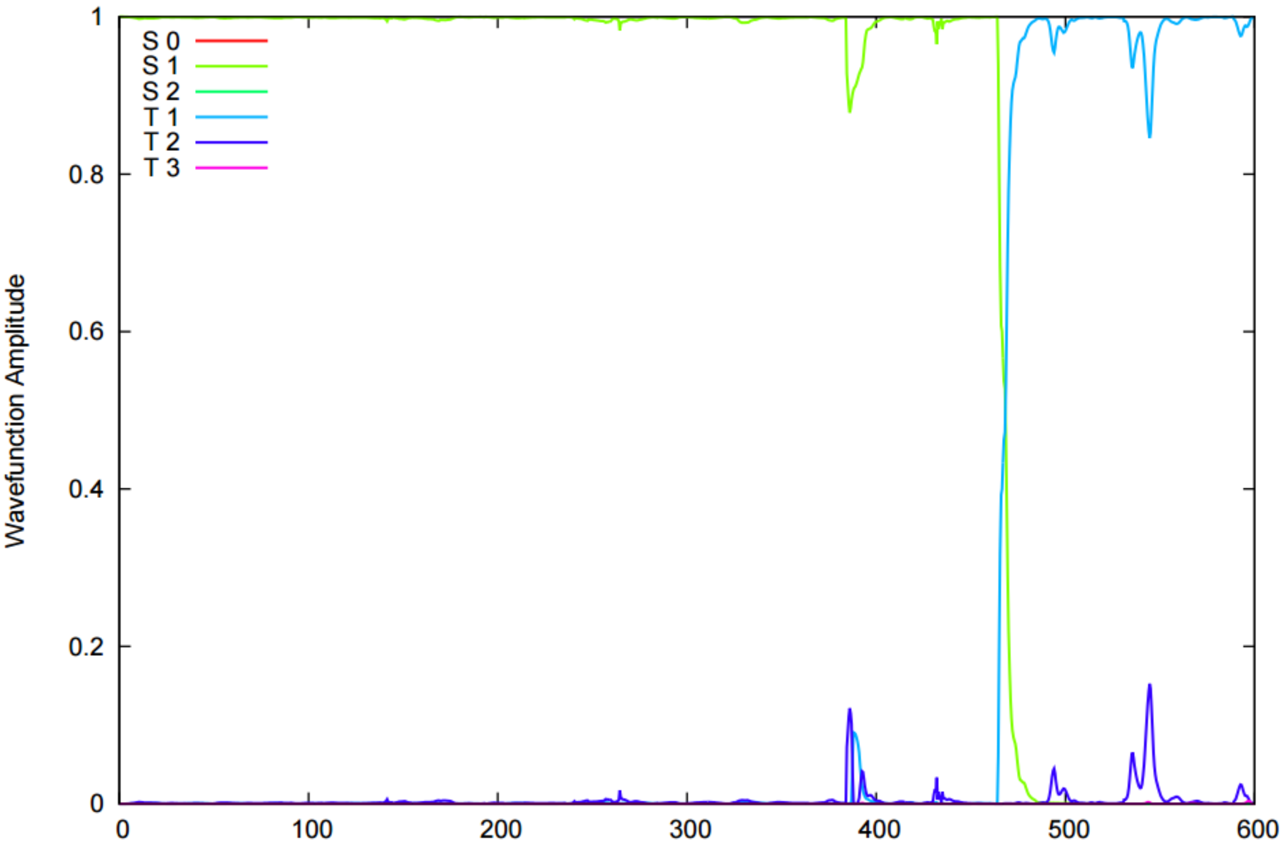
S 0
S 1
S 2
T 1
T 2
T 3
Wavefunction Amplitude
0
0.2
0.4
0.6
0.8
1
0
100
200
300
400
500
600

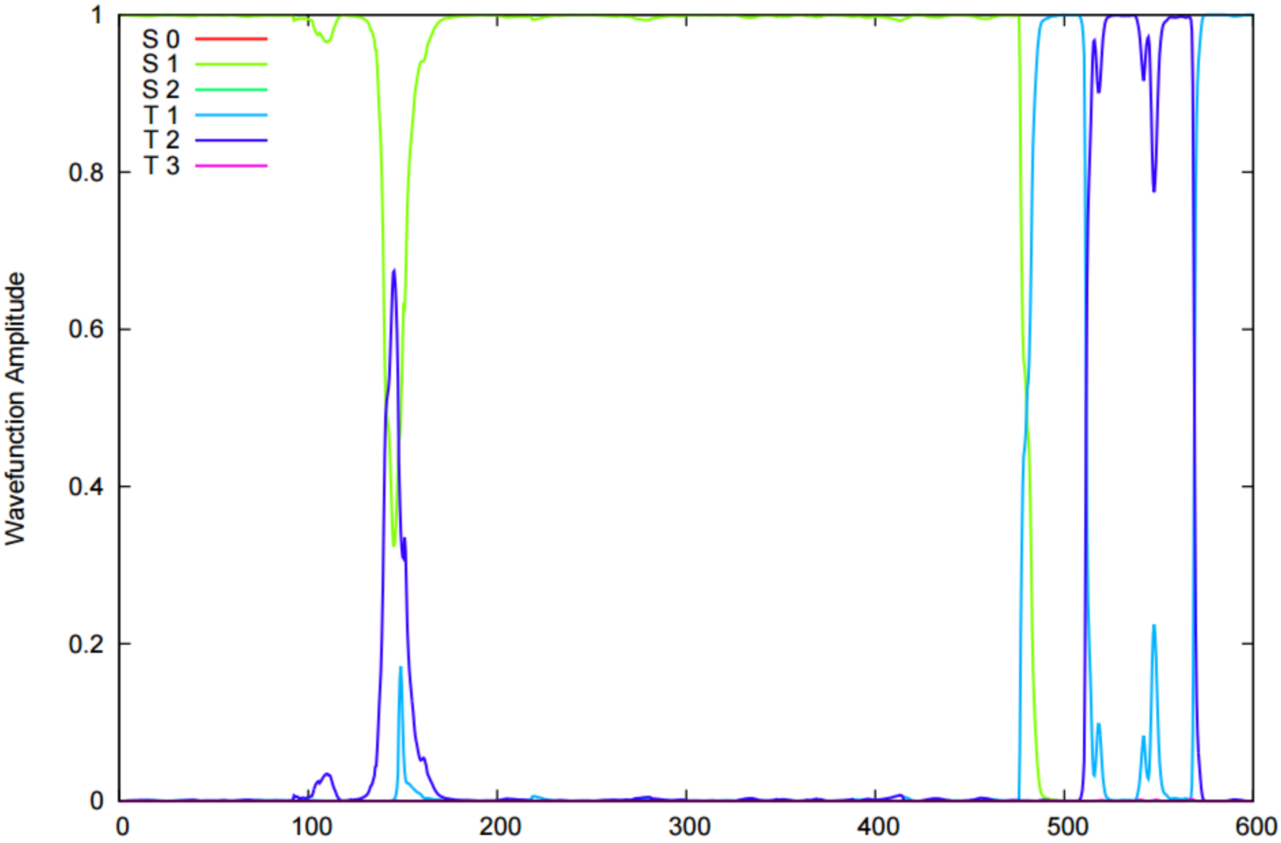
S 0
S 1
S 2
T 1
T 2
T 3
Wavefunction Amplitude
0
0.2
0.4
0.6
0.8
1
0
100
200
300
400
500
600

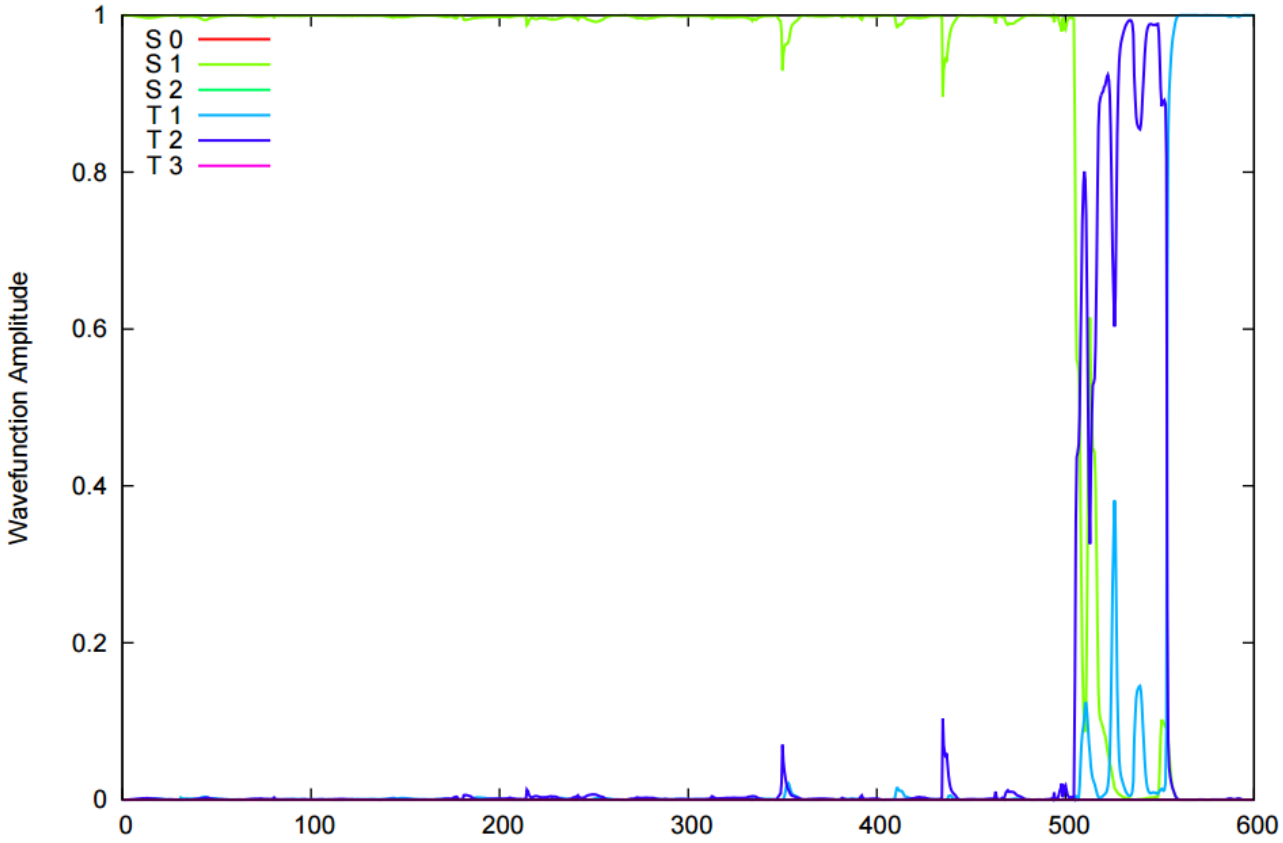
S 0
S 1
S 2
T 1
T 2
T 3
Wavefunction Amplitude
1
0.8
0.6
0.4
0.2
0
0
100
200
300
400
500
600

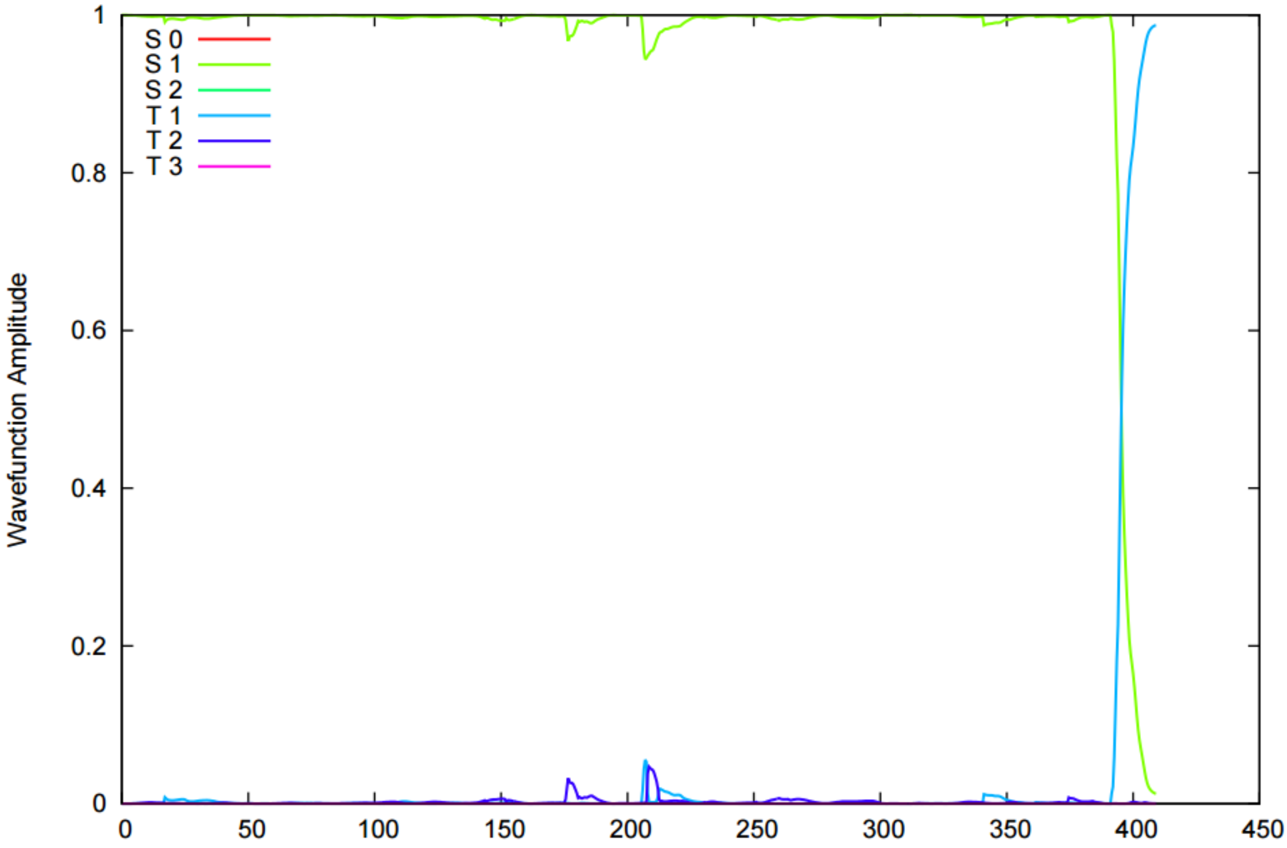
S 0
S 1
S 2
T 1
T 2
T 3
Wavefunction Amplitude
1
0.8
0.6
0.4
0.2
0
0
50
100
150
200
250
300
350
400
450

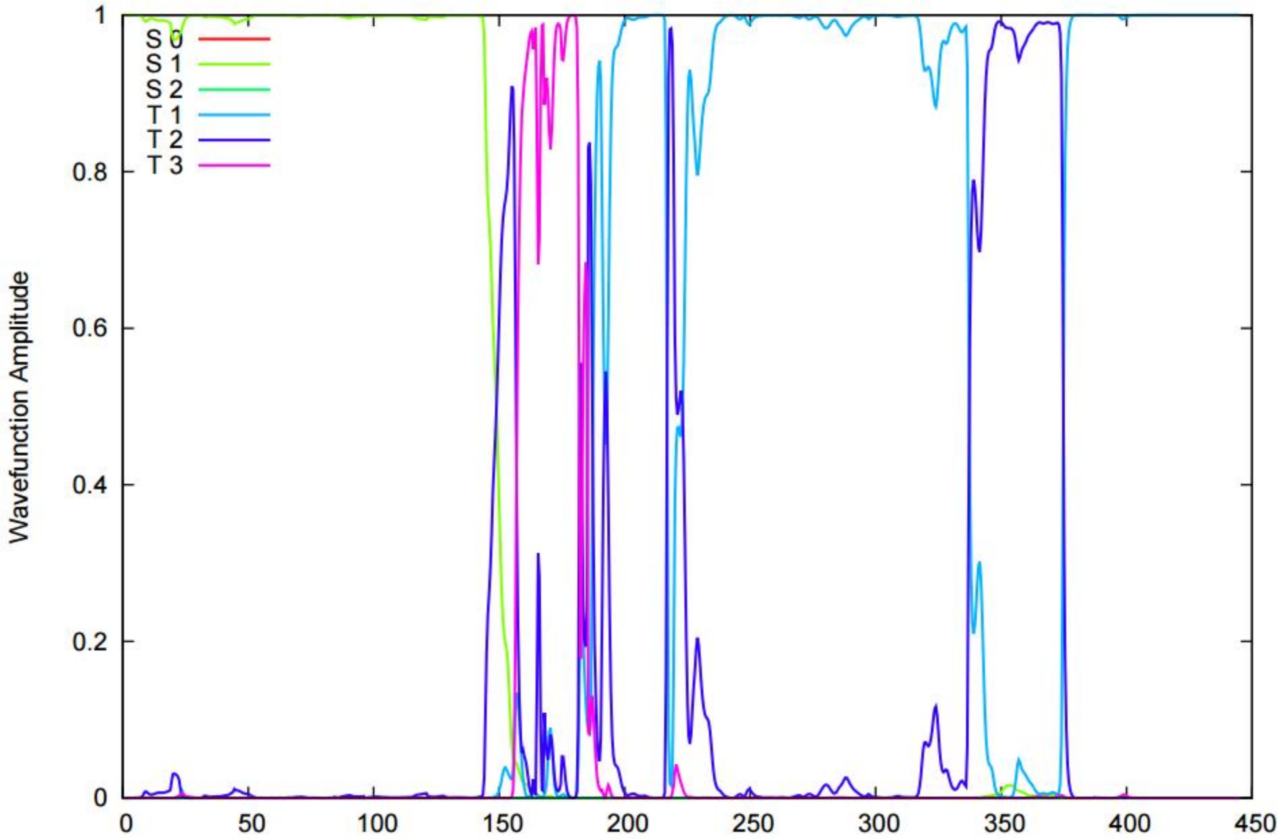
Wavefunction Amplitude
S 0
S 1
S 2
T 1
T 2
T 3
0
0.2
0.4
0.6
0.8
1
0
50
100
150
200
250
300
350
400
450

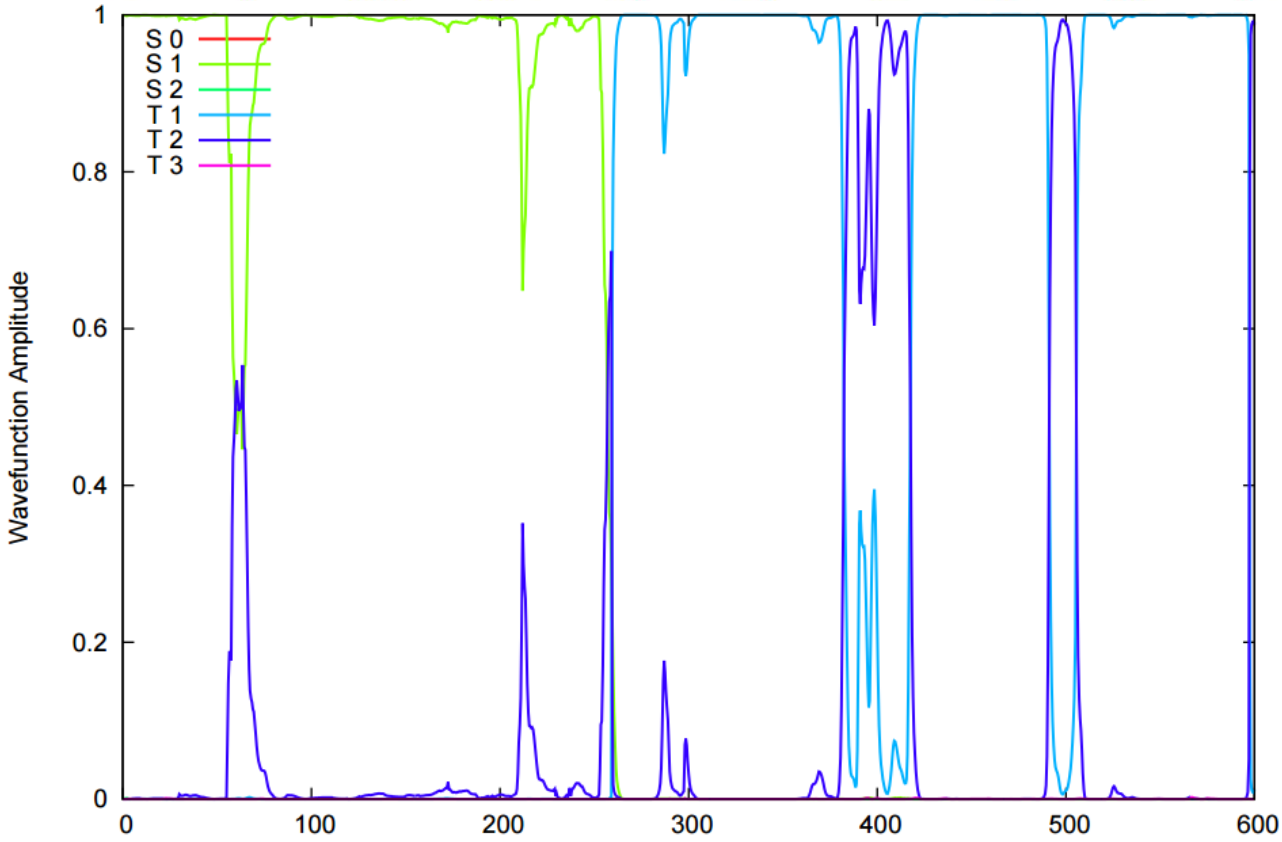
Wavefunction Amplitude
S 0
S 1
S 2
T 1
T 2
T 3
0
0.2
0.4
0.6
0.8
1
0
100
200
300
400
500
600

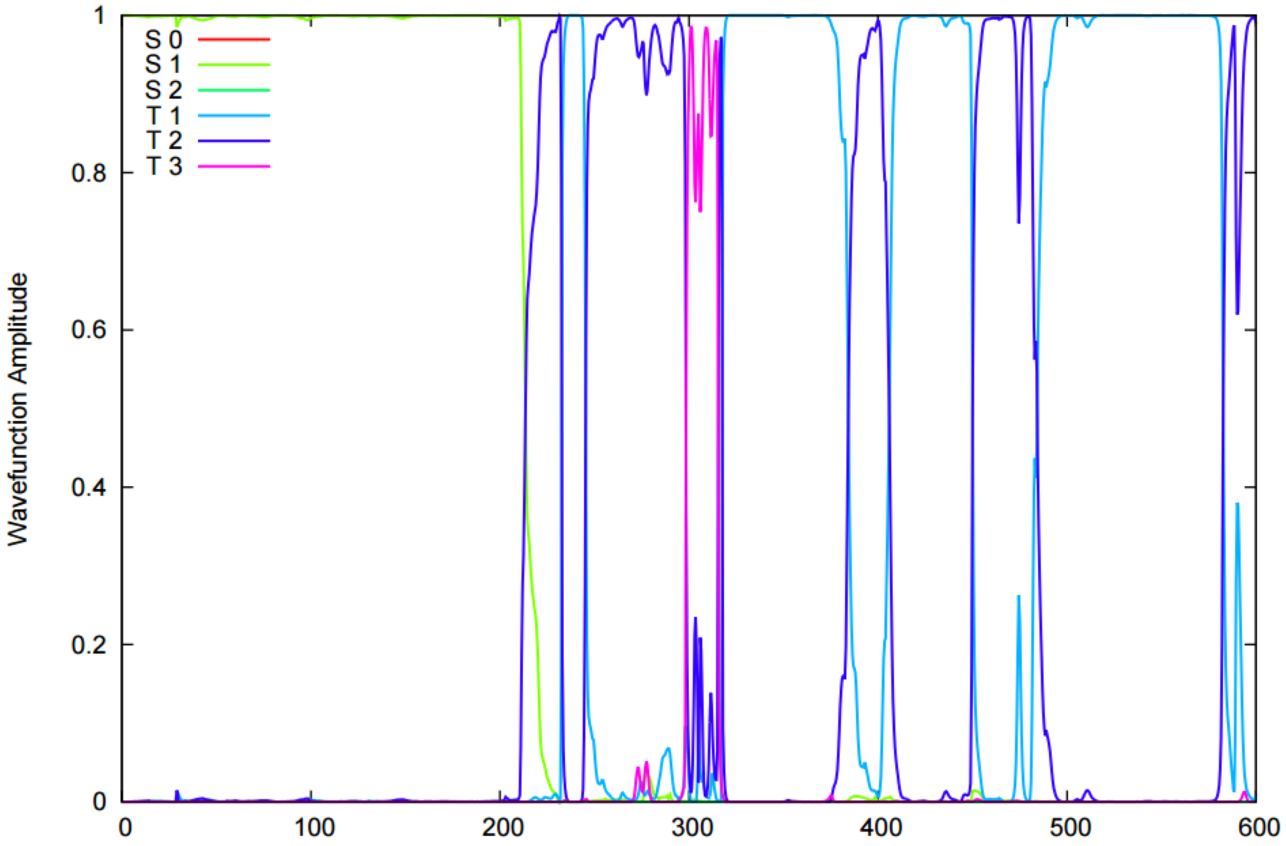
Wavefunction Amplitude
1
0.8
0.6
0.4
0.2
0
0
100
200
300
400
500
600
S 0
S 1
S 2
T 1
T 2
T 3

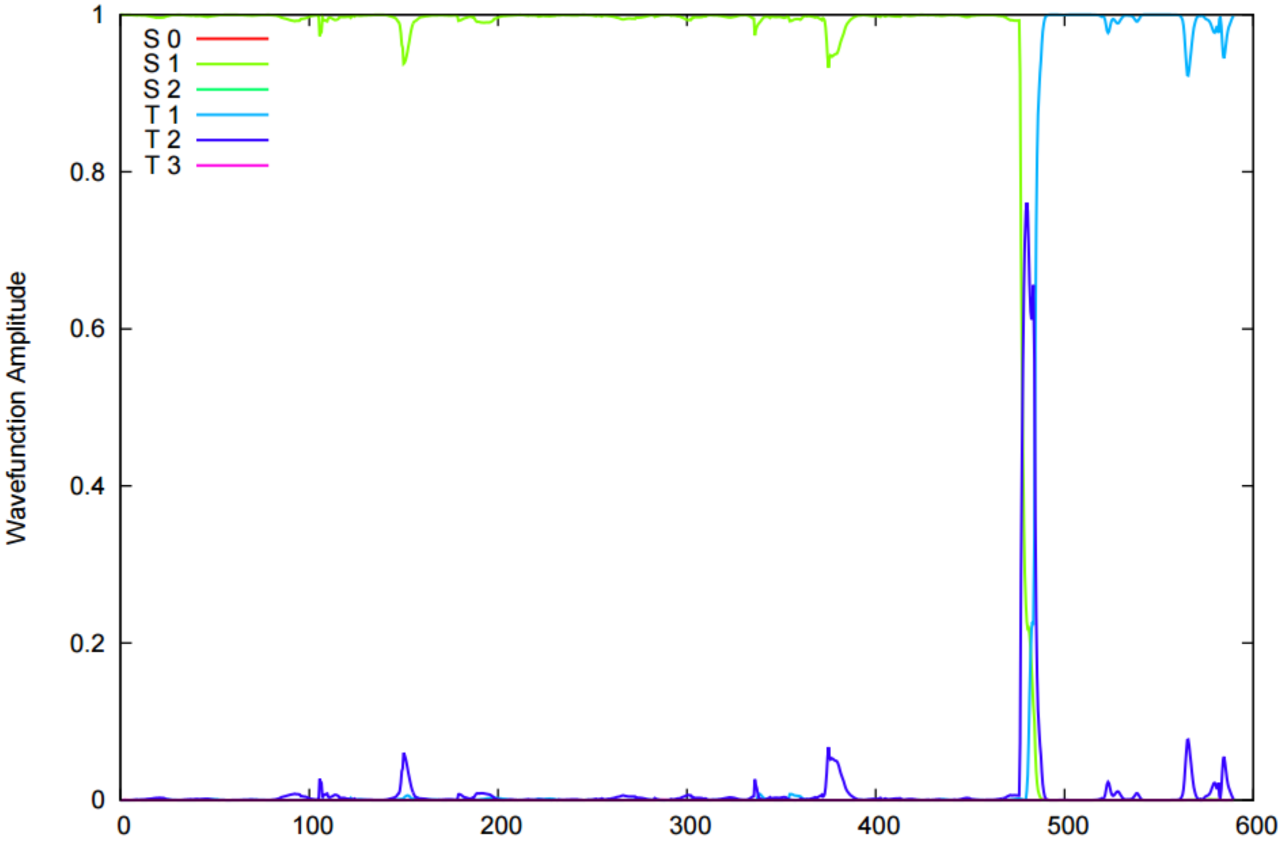
Wavefunction Amplitude
1
0.8
0.6
0.4
0.2
0
0
100
200
300
400
500
600
S 0
S 1
S 2
T 1
T 2
T 3

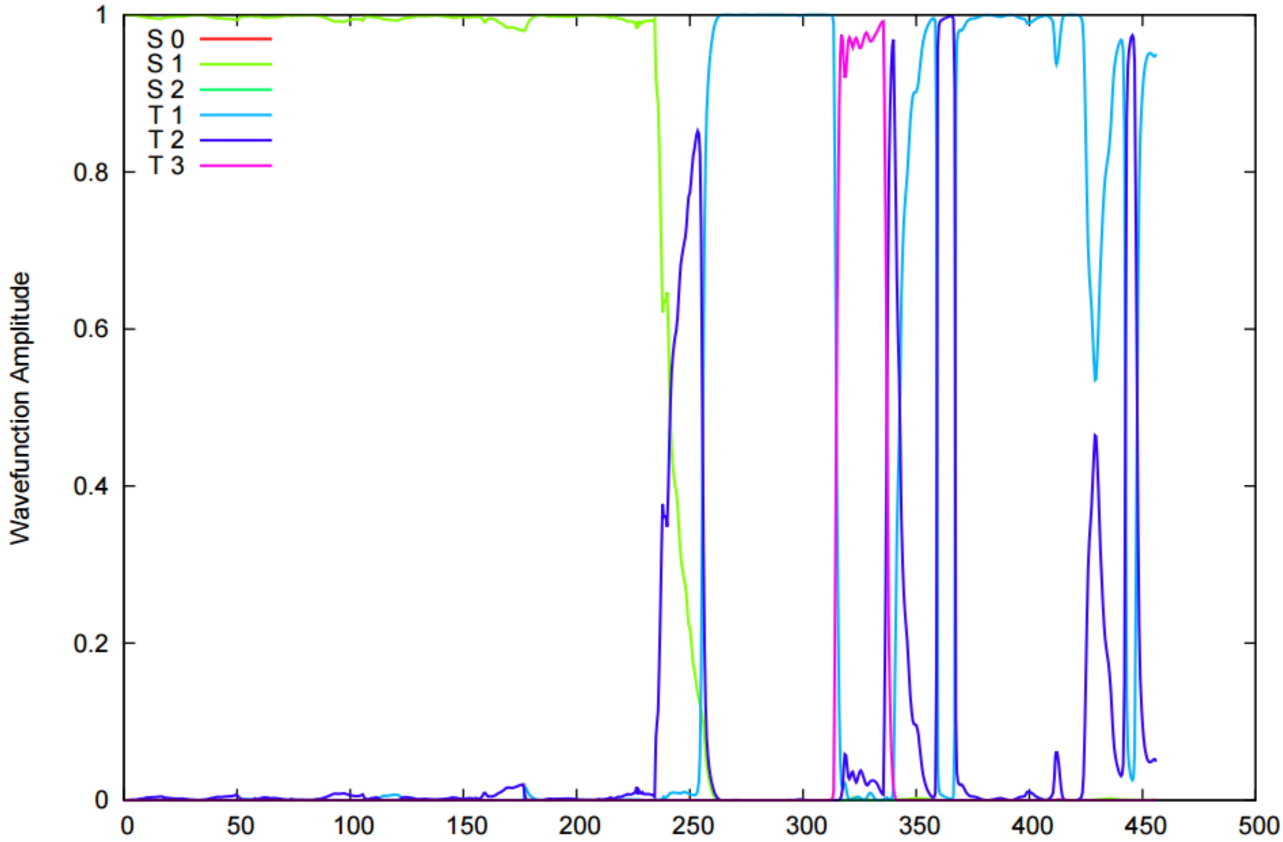
Wavefunction Amplitude
S 0
S 1
S 2
T 1
T 2
T 3
0
0.2
0.4
0.6
0.8
1
0
50
100
150
200
250
300
350
400
450
500

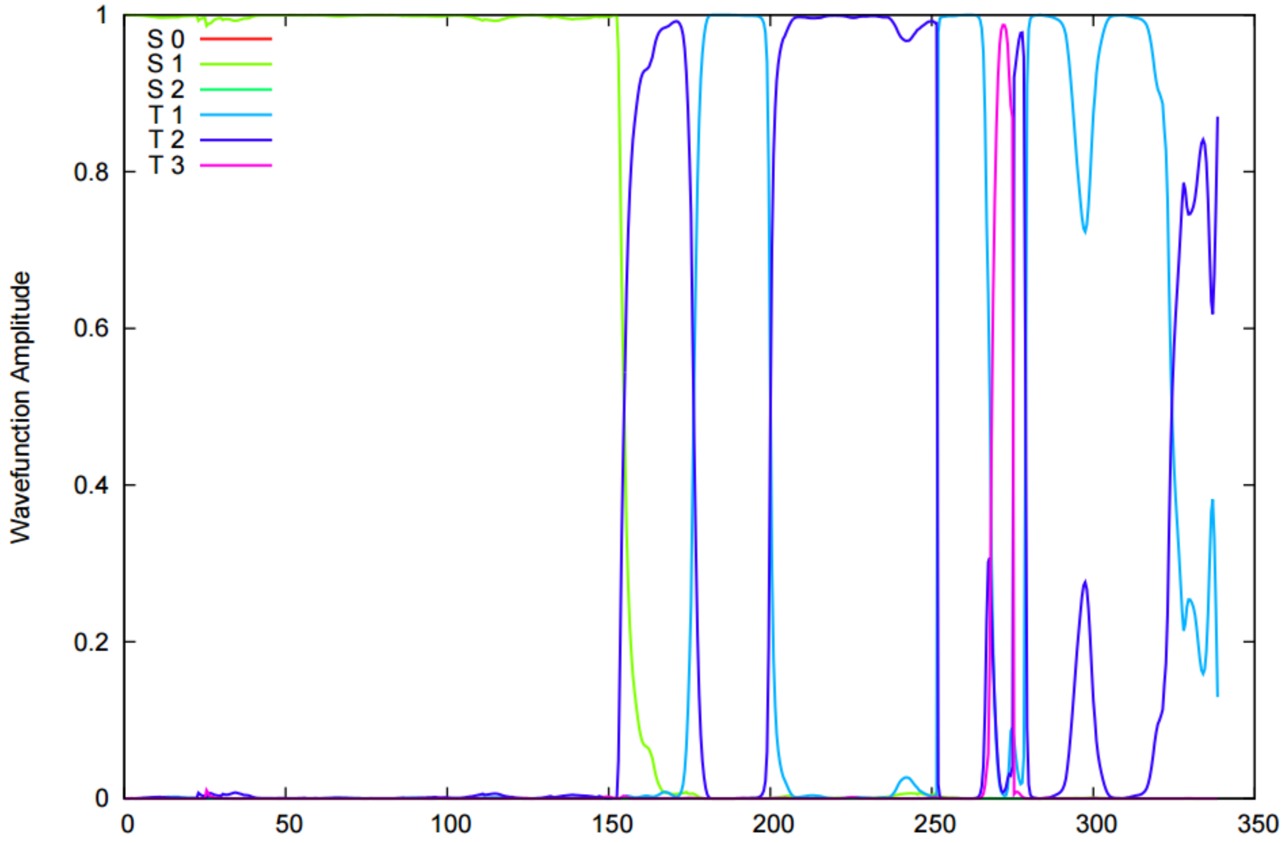
Wavefunction Amplitude
S 0
S 1
S 2
T 1
T 2
T 3
0
0.2
0.4
0.6
0.8
1
0
50
100
150
200
250
300
350

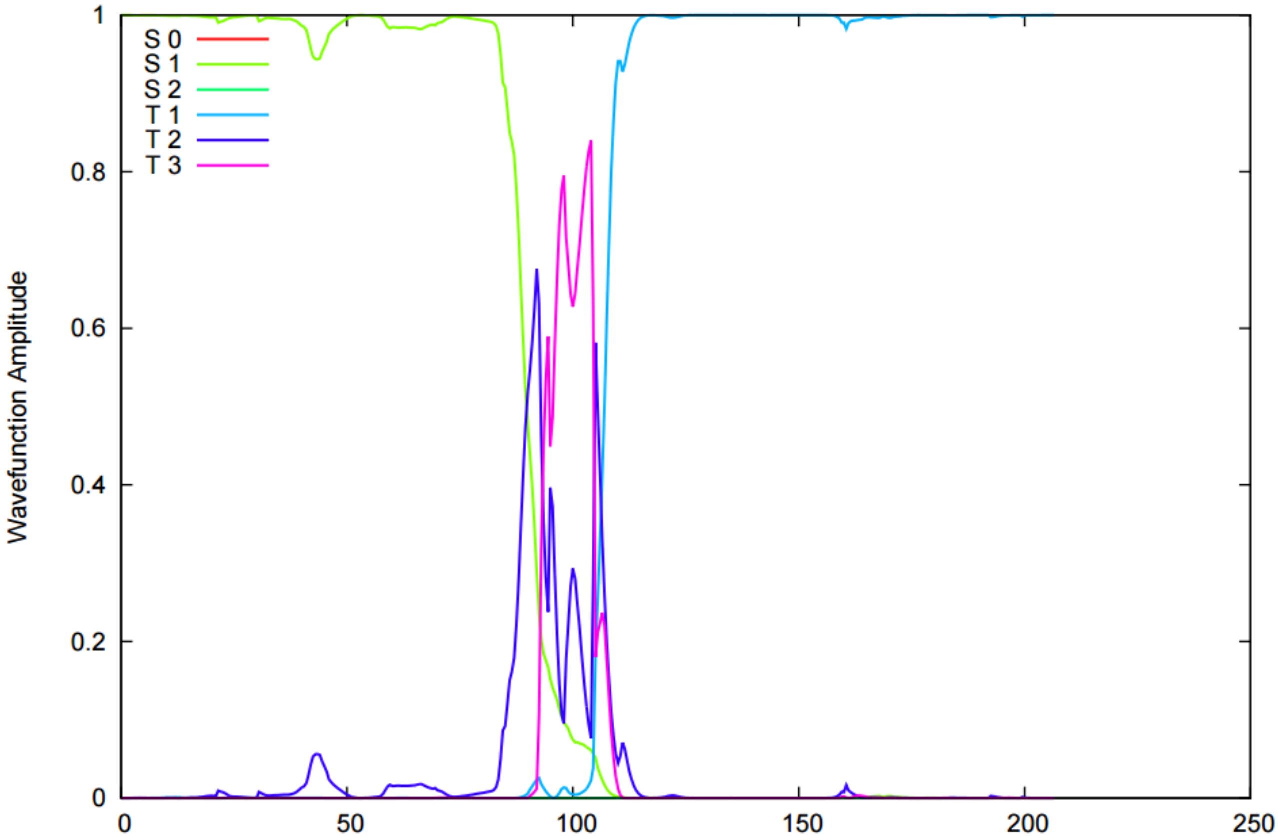
Wavefunction Amplitude
S 0
S 1
S 2
T 1
T 2
T 3
0
0.2
0.4
0.6
0.8
1
0
50
100
150
200
250

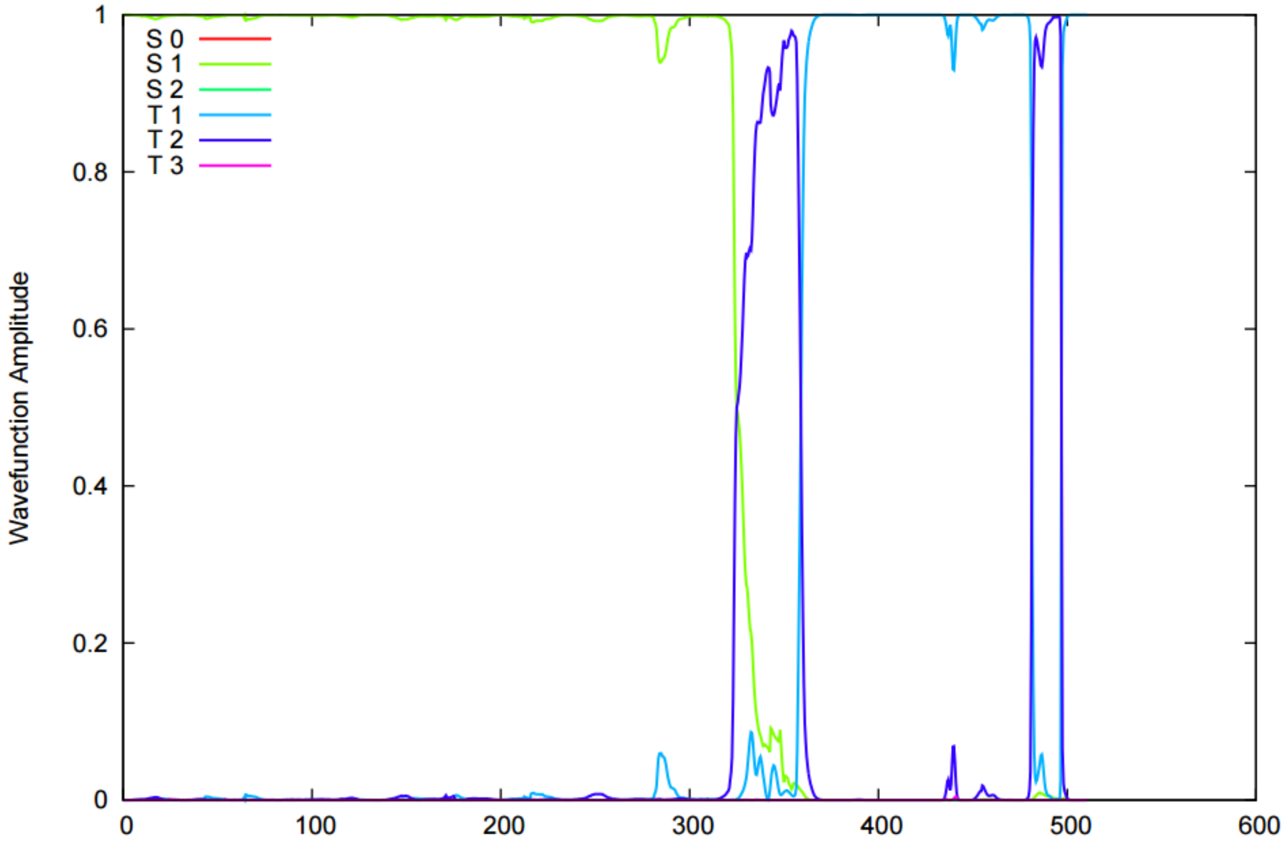
Wavefunction Amplitude
S 0
S 1
S 2
T 1
T 2
T 3
0
0.2
0.4
0.6
0.8
1
0
100
200
300
400
500
600

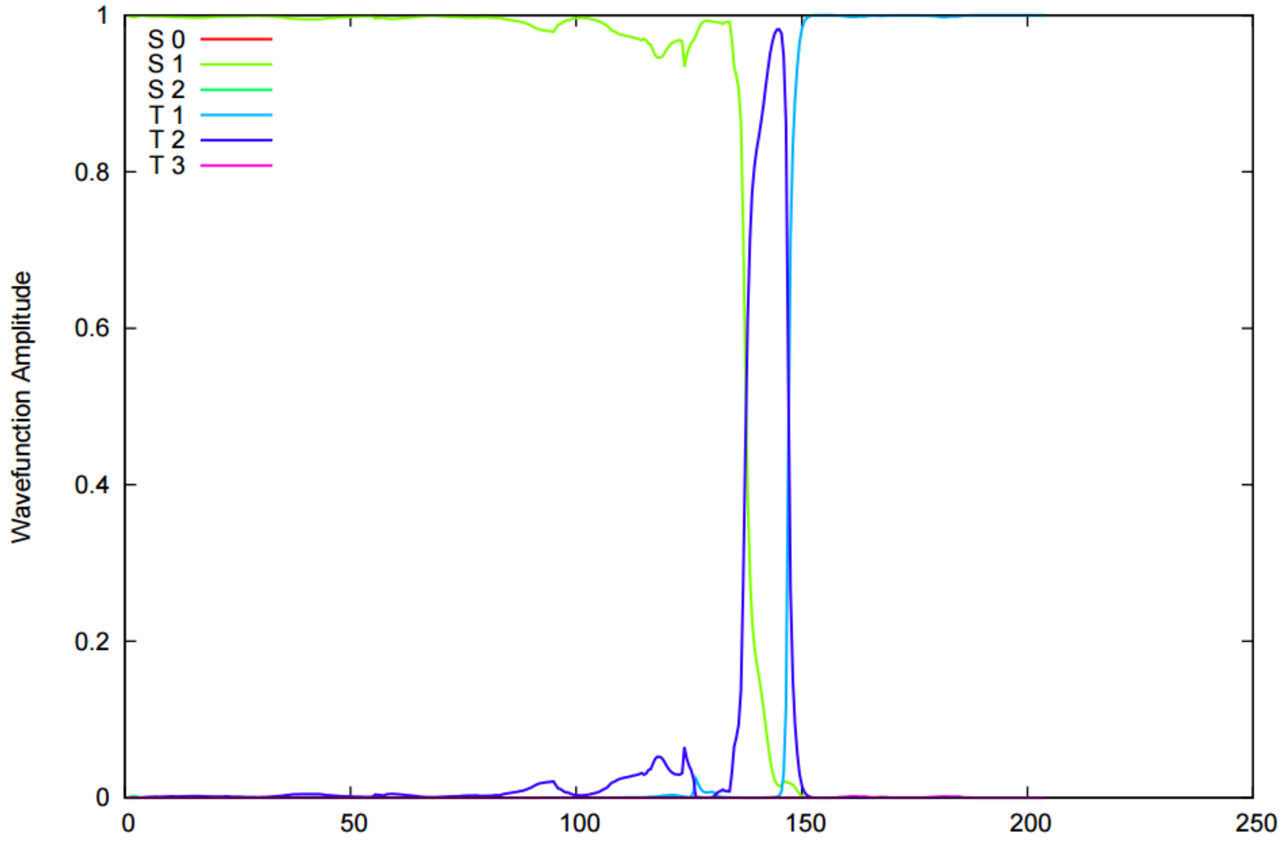

5. Geometrical analysis of the 39 Trajectories Populating the Triplet Manifold

A geometrical analysis was performed, showing the evolution of d_{CO}, Φ_{plan} and θ_{pyr} (see Scheme 1 in the main text) with time.

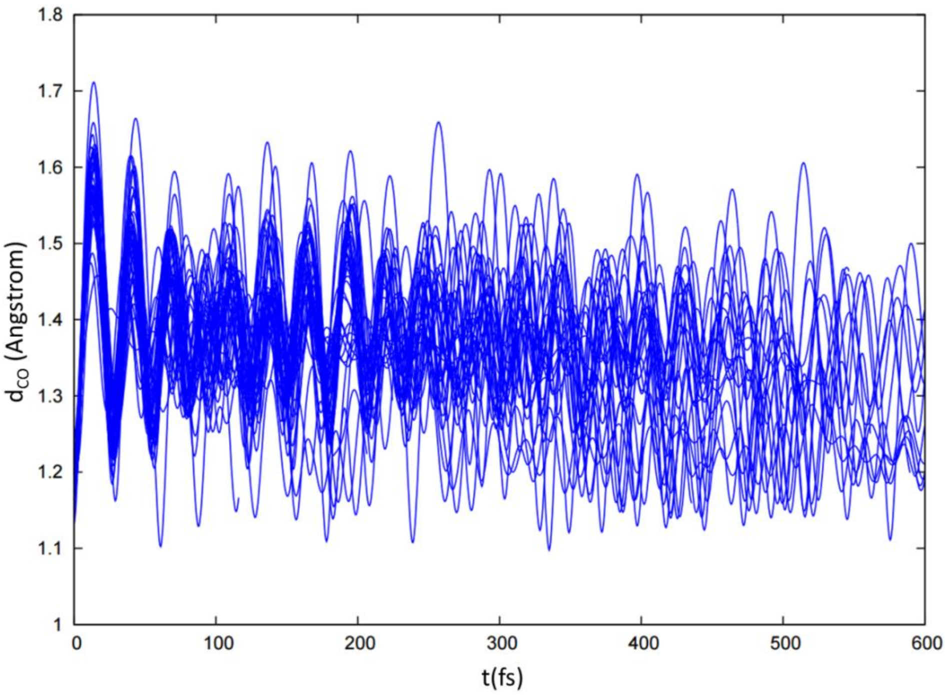

Figure S4. Distance d_{CO} as a function of time.

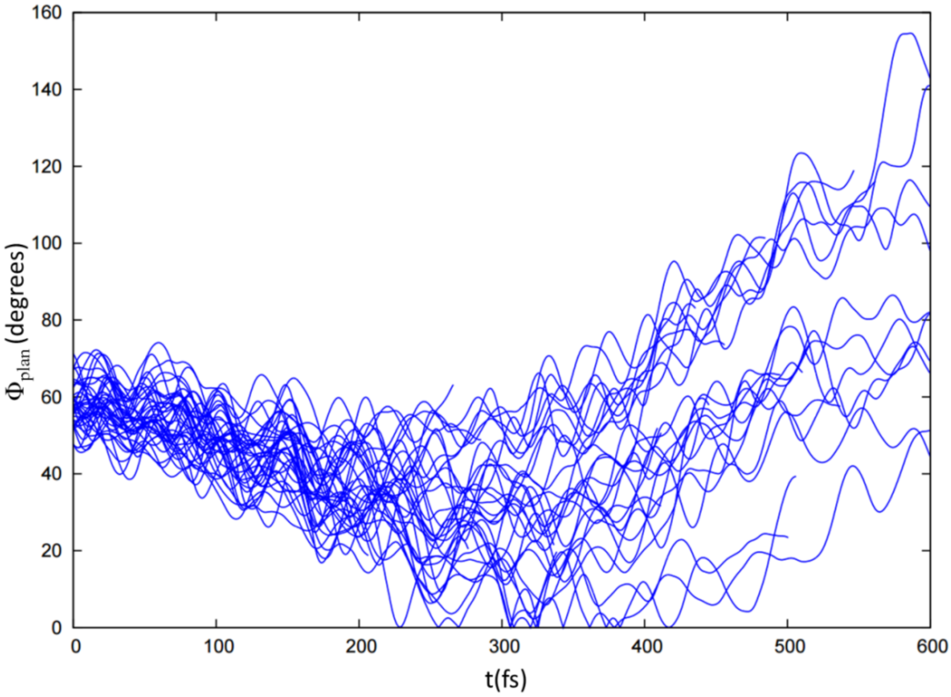

Figure S5. Improper dihedral Φ_{plan} as a function of time.

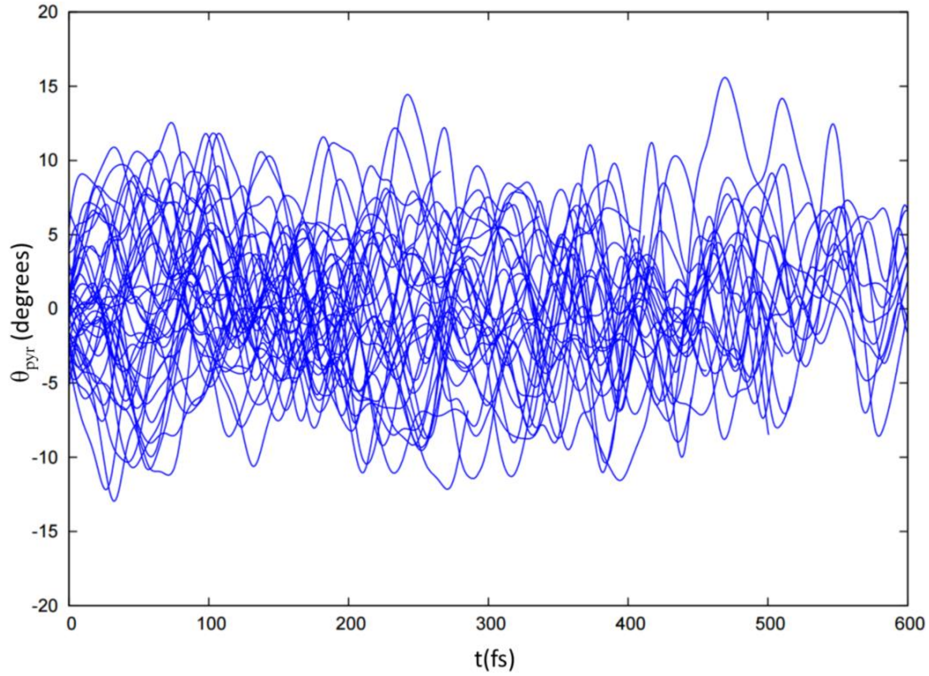

Figure S6. Improper dihedral θ_{pyr} as a function of time.

6. Franck–Condon Structure at the CASSCF(12,11)/ANO-S-VDZP Level of Theory

Cartesian coordinates of the ground state minimum (in Ångström):

24

C	-1.437543	0.739091	0.859277
C	1.430805	-0.703478	0.858942
C	-2.684610	0.798854	1.491329
C	2.660612	-0.788374	1.485356
C	-3.790471	0.162992	0.920526
C	3.784601	-0.191861	0.912147
C	-3.652616	-0.520432	-0.294429
C	3.669564	0.479583	-0.306386
C	-2.414482	-0.561878	-0.936289
C	2.432524	0.547146	-0.948763
C	-1.296571	0.056350	-0.355331
C	1.303991	-0.033908	-0.361696
C	0.002911	0.025596	-1.109938
O	-0.000459	0.048129	-2.303029
H	-0.589003	1.234646	1.303966
H	0.569557	-1.169109	1.311572
H	-2.788778	1.338370	2.422335
H	2.749257	-1.319349	2.423252
H	-4.751691	0.202048	1.414177
H	4.742002	-0.253523	1.410929
H	-4.507152	-1.010193	-0.740270
H	4.537841	0.941035	-0.755685
H	-2.300541	-1.066403	-1.883337
H	2.330253	1.044667	-1.900693

7. Description of the Transient Absorption Spectrum Simulation

The transient absorption spectrum (see Figure 2c in the main text) was simulated directly from non-adiabatic dynamics. For each trajectory at each time step we considered vertical energy differences from the current diagonal state to all the other states. Oscillatory strengths between current state and all the other electronic states, *i.e.* absorption or emission intensity, were directly calculated by the MOLCAS software. Oscillatory strengths were set negative for transition to lower energy states as compared to the current state, and positive elsewhere. This in turn simulates stimulated emission and excited state absorption, respectively. The set of vertical transitions, in eV, was convoluted in the energy domain placing a Gaussian function of full-width at half-length (FWHL) of 0.1 eV, and subsequently converted to nm. Regrouping all the results for all the time steps in a single matrix gave the final map, plotted with the gnuplot program.

We note that this procedure corresponds to the calculation of only the inhomogeneous part of the transient absorption spectrum, since it is based on only the energy gaps between electronic states. In order to include the homogeneous component of the transient absorption spectrum, the calculation of the dynamical Franck–Condon factors would be required.[S13,S14]

Concerning the interpretation of the transient absorption spectroscopy experiments, we note that for both − FC and S_1 minimum − geometries T_3 is higher in energy at the CASSCF level than at the CASPT2 level. Nevertheless, as also mentioned by Sergentu et al. (ref. 21 of the main text), at the CASPT2 level in the FC region the SOC value between S_1 and T_3 was found to be not significant, while SOC values of 24 and 22 cm^{-1} were found for S_1-T_2 and S_1-T_1 states, respectively (ca. 20 cm^{-1} in our study). Therefore, the fact that T_3 is high in energy at FC should not affect the reactivity observed in our study, where T_3 never plays a significant role.

The same holds for the S_1 minimum energy region, since in this case our trajectories are populating the singlet manifold, and therefore they are not used for the interpretation of the transient absorption spectroscopy experiments, that do imply population of the triplet manifold.

As can be seen in Figures 5 and 7 of ref. 21 main text, the CASPT2 MEP predicts that the T_2-T_3 almost degeneracy is left when evolving from FC to the S_1-T_1-T_2 crossing region, corresponding to our T_1-T_2 dynamic equilibrium. In this case, T_3 rises in energy, at both CASSCF and CASPT2 levels of theory. Our considerations about the interpretation of transient absorption spectroscopy experiments do not refer to the FC region, but after triplet population, when finally T_1 and T_2 are almost degenerate and T_3 is indeed upper in energy. Therefore, even considering CASSCF deficiencies, we expect an almost identical T_1-T_3 and T_2-T_3 energy difference (once the triplet manifold is populated and T_1-T_2 equilibrium established). Hence, since $T_1 \rightarrow T_3$ corresponds to a (n,π*) transition and $T_2 \rightarrow T_3$ corresponds to a (π,π*) transition, the $T_2 \rightarrow T_3$ transition results in an optically much brighter (higher oscillator strength) transition than the $T_1 \rightarrow T_3$ transition.

8. References

[S1] Roos, B. O. *Advanced Chemistry and Physics: Ab Initio Methods in Quantum Chemistry II*, ed Lawley KP (Wiley, Chicester, UK), pp 399–445, 1987.

[S2] F. Aquilante, J. Autschbach, R. K. Carlson, L. F. Chibotaru, M. G. Delcey, L. De Vico, I. Fdez. Galván, N. Ferré, L. M. Frutos, L. Gagliardi, M. Garavelli, A. Giussani, C. E. Hoyer, G. Li Manni, H. Lischka, D. Ma, P. Å. Malmqvist, T. Müller, A. Nenov, M. Olivucci, T. B. Pedersen, D. Peng, F. Plasser, B. Pritchard, M. Reiher, I. Rivalta, I. Schapiro, J. Segarra-Martí, M. Stenrup, D. G. Truhlar, L. Ungur, A. Valentini, S. Vancoillie, V. Veryazov, V. P. Vysotskiy, O. Weingart, F. Zapata, R. Lindh. *J. Comput. Chem.* **2015**, *DOI:* 10.1002/jcc.24221.

[S3] P. Å. Malmqvist, B: O. Roos, B. Schimmelpfennig. *Chem. Phys. Lett.* **2002**, *357*, 230-240.

[S4] J. P. Dahl, M. Springborg *J. Chem. Phys.* **1988**, *88*, 4535-4547.

[S5] R. Schinke *Photodissociation Dynamics: Spectroscopy and Fragmentation of Small Polyatomic Molecules* (Cambridge University Press), 1995.
[S6] S. Mai, P. Marquetard, L. Gonzalez. *Int. J. Quant. Chem*. **2015**, *15,* 1215-1231.
[S7] G. Granucci, M. Persico, A. Toniolo. *J. Chem. Phys.* **2001**, *114*, 10608-10615.
[S8] G. Granucci, M. Persico. *J. Chem. Phys.* **2007**, *126*, 1341147.
[S9] T. J. Martinez, M. Ben-Nun, R. D. Levine *J. Phys. Chem.* **1996**, *100*, 7884-7895.
[S10] G. Granucci, M. Persico, A. Zoccante *J. Chem. Phys.* **2010**, *133*, 134111.
[S11] J. E. Subotnik, N. Shenvi *J. Chem. Phys.* **2011**, *134*, 024105.
[S12] J. E. Subotnik *J. Phys. Chem. A* **2011**, *115*, 12083-12096.
[S13] J. G. Saven, J. L. Skinner *J. Chem. Phys.* **1993**, *99*, 4391.
[S14] A. S. Petit, J. E. Subotnik *J. Chem. Phys.* **2014**, *141*, 154108.